

ABSTRACT

Design of a Microwave Sensor for Non-Invasive Determination of Blood-Glucose Concentration

Eric C. Green

Mentor: B. Randall Jean, Ph.D.

Diabetes is a disease that afflicts millions worldwide. To control the effects of this disease, diabetics must check their blood glucose levels on a regular basis. Currently, all daily glucose monitoring techniques are invasive, requiring a sample of blood.

Microwave sensors are non-destructive and non-contact measuring devices, making them ideal for the measurement of parameters in industrial processes. Current uses of microwave sensors range from measuring moisture content of corn chips to measuring concentration of a solute in water. If a microwave sensor were developed to determine blood glucose concentration, it could be the first daily-use glucose-measuring technique that is truly non-invasive.

This thesis provides background on diabetes and microwave measurement. From this background, a sensor is developed and its advantages are illustrated. The thesis concludes by making suggestions for improving the sensor and recommendations on how to implement the sensor into a useful product.

Design of a Microwave Sensor for Non-Invasive Determination of
Blood Glucose Concentration

by

Eric C. Green, B.S.

A Thesis

Approved by the Department of Electrical and Computer Engineering


James B. Farison, Ph.D., Chairperson

Submitted to the Graduate Faculty of
Baylor University in Partial Fulfillment of the
Requirements for the Degree
of
Master of Science in Biomedical Engineering

Approved by the Thesis Committee



B. Randall Jean, Ph.D., Chairperson


Robert J. Marks II, Ph.D.


Dennis A. Johnston, Ph.D.


Carolyn T. Skurla, Ph.D.

Accepted by the Graduate School
December 2005


J. Larry Lyon, Ph.D., Dean

Copyright © 2005 by Eric C. Green

All rights reserved

TABLE OF CONTENTS

LIST OF FIGURES	iv
LIST OF TABLES	vii
GLOSSARY	viii
ACKNOWLEDGMENTS	xii
DEDICATION	xiii
CHAPTER ONE	
Introduction.....	1
CHAPTER TWO	
Diabetes, Glucose, and Non-Invasive Measurement	3
CHAPTER THREE	
Microwave Properties and Measurement.....	8
CHAPTER FOUR	
Biology and Microwaves	16
CHAPTER FIVE	
Microwave Properties of Biological Materials	21
CHAPTER SIX	
Design of a Microwave Sensor for Electrical Characterization of Biological Materials from 50 MHz to 2 GHz	32
CHAPTER SEVEN	
Experimental Results from a Single-Spiral Microstrip Resonant Sensor	43
CHAPTER EIGHT	
Final Recommendations and Description for Development of a Non-Invasive Glucose Meter	51
BIBLIOGRAPHY	53

LIST OF FIGURES

Fig. 1: Normal regulation of blood glucose	4
Fig. 2: The electromagnetic spectrum.....	8
Fig. 3: Diagram of a rectangular waveguide.....	10
Fig. 4: Vector Network Analyzer connected to a rectangular waveguide	10
Fig. 5: The field lines for a TE_{10} wave propagating inside a waveguide.....	11
Fig. 6: Field lines for an open-ended coaxial probe.....	12
Fig. 7: The Agilent High Temperature Dielectric Probe	13
Fig. 8: Ring resonator circuit.	14
Fig. 9: Output plot for a ring resonator circuit.....	14
Fig. 10: Bowtie antenna developed for microwave mammography.....	18
Fig. 11: Bowtie-slot antenna used in microwave plethysmography.....	19
Fig. 12: Idealized dispersion regions for tissue	21
Fig. 13: Dielectric properties of body tissues	22
Fig. 14: Relative dielectric constant of certain tissues.....	24
Fig. 15: Relative dielectric constant of certain tissues.....	24
Fig. 16: Influence of D-glucose on dielectric constant of erythrocyte suspension.....	27
Fig. 17: Suggested mechanism for change in cell membrane.....	27
Fig. 18: Plots for (a) dielectric constant at 10 kHz and (b) the hamster's blood	28
Fig. 19: Layout for non-invasive impedance spectroscopy glucometer	29
Fig. 20: Glucose profiles measured invasively, and with dielectric spectroscopy	30
Fig. 21: Layers of the simulated sensor load.	34

Fig. 22: Second order Debye model of blood used in sensor testing.....	35
Fig. 23: Microstrip Ring Resonator modeled in CST Microwave Studio	36
Fig. 24: Response of the Microstrip Ring Resonator.....	36
Fig. 25: Slotline Ring Resonator modeled in CST Microwave Studio.....	37
Fig. 26: Response of the Slotline Ring Resonator	37
Fig. 27: Microstrip Clover Resonator modeled in CST Microwave Studio	38
Fig. 28: Response of the Microstrip Clover Resonator.....	38
Fig. 29: Slotline Clover Resonator modeled in CST Microwave Studio.....	39
Fig. 30: Response of the Slotline Clover Resonator	39
Fig. 31: Dual-Spiral Microstrip Resonator modeled in CST Microwave Studio	40
Fig. 32: Response of the Dual-Spiral Microstrip Resonator.....	40
Fig. 33: Single-Spiral Microstrip Resonator modeled in CST Microwave Studio	41
Fig. 34: Response of the Single-Spiral Microstrip Resonator	41
Fig. 35: Surface currents on the single-spiral at 1.5 GHz.....	42
Fig. 36: Front and back view of main layer project board.....	43
Fig. 37: Front and back view of secondary layer project board.....	43
Fig. 38: The sensor feed structure and the completed sensor	44
Fig. 39: $ S_{11} $ and $ S_{21} $ for air, ultem, and tile.....	45
Fig. 40: $ S_{11} $ and $ S_{21} $ for various temperatures of water	46
Fig. 41: $ S_{11} $ and $ S_{21} $ response of sensor loaded with meat.....	47
Fig. 42: Tracking a local minimum vs. fat content in $ S_{11} $ and $ S_{21} $	47
Fig. 43: Sensor located at the wrist measuring-site	48
Fig. 44: $ S_{21} $ plots from each measurement taken over the duration of the soda test..	48

Fig. 45: Tracking a maximum of the $ S_{21} $ over time	50
Fig. 46: Tracking a minimum of the $ S_{11} $ over time	50

LIST OF TABLES

Table 1: IEEE recommendations for SAR of electromagnetic energy	16
Table 2: Parameters of the Cole-Cole model for certain tissues.....	25
Table 3: Compiled results for sensors designed in this thesis	35

GLOSSARY

A, B – Constants used in the load admittance calculation for an open-ended coaxial probe.

ATP – Energy used in the body by cells, adenosine tri-phosphate.

c – The speed of light (300×10^8 cm/s).

C_l, C_0 – Capacitance values used in the load admittance calculation for an open-ended coaxial probe.

CAT Scan – Computed Axial Tomography, used as a means for imaging tissues inside the body.

Coupling Gap – A gap in a microwave structure where energy is coupled from one feature to another.

CST Microwave Studio – A microwave modeling software package created and distributed by CST (Computer Simulation Technology). All modeling in this thesis was done in version 5.1.1 of the software.

Diabetes – A disease where the body does not properly regulate glucose.

Diathermy – The process of heating tissue with electromagnetic energy, often used in medicine as a treatment. Also called hyperthermia.

Dielectric Constant – The real part of permittivity, ϵ' .

Dispersion – Region of decreasing dielectric constant.

Erythrocyte – A red blood cell, the most abundant non-water component in the blood.

FDA – United States Food and Drug Administration.

FR4 – The dielectric material used in this thesis to separate ground planes from signal carrying traces which has a relative dielectric constant of 4 at microwave frequencies.

Glucometer – A tool used to measure blood glucose.

Glucose – A biological sugar that is the body's power source.

Hyperglycemia – When the concentration of glucose in one's body rises too high.

Hypoglycemia – When the concentration of glucose in one's body falls too low.

IEEE – A professional organization for electrical engineers called the Institute of Electrical and Electronics Engineers

in vitro – Outside the body.

in vivo – Inside the body.

Insulin – Hormone used to break down glucose in the body.

Ketones – Acidic byproduct of hyperglycemia.

Loss Factor – The imaginary part of permittivity, ϵ'' .

MAML – The Microwave Applied Metrology Lab at Baylor University.

Maxwell-Wagner Interfacial Polarizations – Polarizations in biological tissues that occur at low frequencies and contribute to the high dielectric constant of biological materials.

Microwave – A radio wave between 100 MHz and 100 GHz.

Microwave Thermography – The process of measuring temperature inside a body as a function of passive thermal radiation given off by that body.

MRI – Magnetic Resonance Imaging, used as a means for imaging tissues inside the body.

MUT – The material under test, or a material being tested by a system.

MWS – CST Microwave Studio

Open-ended Coaxial Probe – A contact sensor used to measure electrical permittivity as a function of the signal reflected by the MUT.

Permittivity, ϵ – A measure of how much electrical energy a material stores and dissipates when it is in an electric field.

Plethysmography – The practice of measuring certain physiological parameters to estimate the size of an organ.

r – The radius of a microwave ring resonator.

Rectangular Waveguide – A metal box, open at one or both ends, used to measure electrical permittivity of materials.

Relative Permittivity, ϵ_r – A unitless ratio of the permittivity of an object to the permittivity of free space.

Resonant Sensor – A means for measuring a material's permittivity by sensing shifts in S-parameters due to loading by the MUT.

S11 – The response of a sensor at port 1 as a result of a signal input at that port, reflection.

S21 – The response of a sensor at port 2 as a result of a signal input at port 1, transmission.

SAR – Specific Absorption Rate, a value related to the absorption of electromagnetic energy.

Slotline – A microwave transmission structure created by etching traces into a plane of conducting material; the signal is launched into the void between the remaining conductors. The slotlines in this thesis are etched into a layer of copper which is on top of substrate; there is a ground plane on the substrate opposite the slotline.

Stripline – A microwave transmission structure that consists of a trace between two ground planes, separated by a substrate. This structure is able to support a perfectly TEM wave.

T – The transmission coefficient.

TE₁₀ Mode – The lowest frequency transverse electric mode of a wave in a waveguide.

TEM Wave – Transverse Electromagnetic wave; a wave where the electric field and magnetic field are orthogonal to each other as well as the direction of propagation.

Ultem – A dielectric material with $\epsilon' = 6$ at microwave frequencies.

VNA – Vector network analyzer, a tool used to determine the S-parameters of a microwave circuit over a frequency range.

$Y_L(\omega, \epsilon)$ – Admittance of a load, dependant on the permittivity of a sample and the angular frequency at which the admittance was measured.

ϵ_{eff} – The effective permittivity is the permittivity value “seen” by a loaded or unloaded microwave sensor.

ϵ_∞ – A material's electric permittivity at extremely high frequencies.

$\Gamma(\omega, \epsilon)$ – The microwave reflection coefficient, dependant on the permittivity of a sample and the angular frequency at which the reflection was measured.

λ_g – Wavelength of a wave on a microstrip ring resonator.

η_i – The intrinsic impedance of a material.

τ_n – a material's time constant, used in the Debye and Cole-Cole equations.

μ – A material's magnetic permeability

ACKNOWLEDGMENTS

Thanks to Dr. Jean for all the “pep talks.” You always helped keep me from getting discouraged. Thanks to my parents for their love and encouragement. You taught me never to settle for “good enough.” And thanks to my bride-to-be Christine. From day one you listened to me ramble about microwaves and glucose without complaining. Your patience and understanding is amazing, and your desire to see me succeed is the best motivator of all!

DEDICATION

To my love Christine – you're my favorite!

CHAPTER ONE

Introduction

Over the past half-century, microwave instruments have been used increasingly in a wide range of sensing applications [1]. Their ability to nondestructively measure parameters inside a volume makes them ideal for measuring in harsh or sensitive environments where direct contact to the sample cannot be achieved. This property of microwave sensors suggests that they would be well suited for non-invasively measuring physiological parameters in humans. One such parameter, and the guiding example for this research, is blood glucose concentration, which diabetics must closely monitor.

Diabetes is a disease that afflicts millions worldwide. It results from the body's improper regulation of the hormone insulin. Insulin is used to break down glucose, a biological sugar that is the body's power source. To be healthy, the body must maintain glucose concentration within a specific range; if the concentration falls out of this range, then permanent damage to vital organs may result. This is why it is important for diabetics to monitor their glucose levels. Unfortunately, most methods currently used by diabetics for determining blood glucose concentration are invasive, requiring direct contact with a sample of blood. The intent of this thesis is to outline the design of a microwave sensor that could be applied to non-invasive determination of blood glucose concentration.

I obtained firsthand knowledge of the methods and techniques that follow working in Baylor University's Microwave Applied Metrology Lab (MAML). Working in the MAML, I have spent a considerable amount of time researching the dielectric

properties of glucose, blood, and other biological tissues. I have also learned the basics of measuring the permittivity of homogeneous material. Much of the knowledge that follows is a direct result of this work. Additionally, the preliminary work supporting this research was documented in my undergraduate honors thesis [2].

CHAPTER TWO

Diabetes, Glucose, and Non-Invasive Measurement

Diabetes affects between four and six percent of the adult population [3]. It is the seventh leading cause of death in the United States. Additionally, 50% of Americans possess one or more symptoms of the disease [4]. In 2002, diabetes cost the citizens of the United States a staggering \$132 billion, up 35% from \$98 billion in 1997 [5]. Annually, nearly 20% of total personal healthcare costs are directly related to diabetes. The cause of some types of diabetes is not known, but studies suggest that an improper diet over a prolonged period may be a direct factor. Given the dietary trends of Americans and the increasing numbers of senior citizens, these figures will continue to rise.

Diabetes comes in two forms, an autoimmune disease or a metabolic disorder, which result from the body's improper regulation of insulin. Insulin is produced by the pancreas (see Fig. 1) and secreted into the bloodstream to manage the blood's concentration of glucose, also called blood sugar. Type 1 diabetes occurs when the pancreas fails to produce proper amounts of insulin. This condition may be present from birth or develop later in life. Type 2 diabetes develops over time. The glucose receptors on the cells of Type 2 diabetics are damaged, and thus the cells no longer use insulin effectively. This condition may be caused by a combination of factors, including poor eating habits, lack of exercise, or genetic predisposition.

Diabetes has no known cure, but may be managed with insulin injections. For Type 1 diabetics, this injection is the insulin the body needs to function; for Type 2

diabetics, the insulin excess inundates the damaged cells and helps them absorb a healthy amount of glucose. The symptoms of diabetes include poor blood circulation, blurred vision, loss of energy, and wounds that are slow to heal [3].

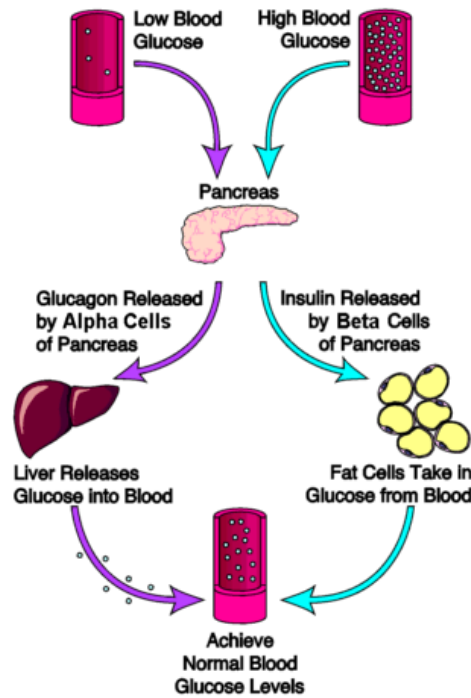


Fig. 1: Normal regulation of blood glucose [6]

Like all processes, biological functions require energy. In the human body, energy comes in the form of glucose, a simple sugar compound. Glucose is transported throughout the body via the bloodstream. Cells then absorb and process the glucose through a process called glycolysis. Therefore, without proper transportation and absorption of glucose, life could not exist.

If the concentration of glucose in one's body rises too high, a condition called hyperglycemia, the body produces ketones [3]. Ketones are acidic, so prolonged exposure to them may damage organs. A frequent side effect of diabetes is kidney

failure, which may result in years of uncomfortable dialysis and an early death. Heart disease is another result of increased ketones.

If the glucose concentration in one's body is too low, a condition called hypoglycemia, cells do not receive enough energy to function. This condition is extremely dangerous and hazardous to the body. At least 50 to 60% of glucose used by the body is consumed in the brain and nervous system [7]. Consequently, during episodes of severe hypoglycemia, a diabetic can slip into a coma which may ultimately cause brain damage or loss of life [3]. Clearly, manual regulation of blood glucose is important for those whose bodies fail to do so properly.

Blood glucose levels vary during a regular day. The acceptable range of glucose concentration is 70 mg/dL to 110 mg/dL. Glucose levels spike shortly after eating and may reach as high as 180 mg/dL but should normalize within two to three hours [6]. When a person's blood sugar takes longer than three hours to return normal, he potentially has diabetes. A diabetic's glucose level must be closely monitored to ensure compliance with the above range. Depending on the severity of the disease, blood glucose concentration must be measured one to four times per day [8]. This measurement is taken with a glucometer, a tool specifically designed for measuring blood glucose. Most glucometers can measure from 0 mg/dL to 600mg/dL with at least 15% accuracy. The American Diabetes Association recommends that a glucometer achieve "variability (system plus user) of 10% at glucose concentrations of 30-400 mg/dL 100% of the time" [9].

The traditional glucometer measures direct samples of blood, typically taken from the fingertip. The user pierces his skin with a lancet and then squeezes his finger until a

substantial amount, usually 1 large drop, of blood has been collected on the appropriate test strip. The strip is then inserted into a glucometer, which determines glucose concentration. Depending on the type of glucometer, reflectance photometry, absorbance photometry, or an electrochemical methodology is used to determine glucose concentration.

All three methods use glucose oxidase, a chemical that when mixed with glucose produces a color change proportional to the amount of glucose in the blood. Units that use reflectance photometry or absorbance photometry bombard the test strip with light and measure the reflected wavelength to determine blood sugar concentration. The electrochemical methodology measures the flow of electrons in amperes produced by the chemical reaction between blood and glucose oxidase [9]. These methods require direct samples of blood which must be obtained by puncturing the skin. Young and old diabetics alike dread this necessary, yet painful, "invasive" method of checking their blood sugar.

Given the prevalence of diabetes, there is a great deal of research aimed at developing a "minimally invasive" or "non-invasive" method for measuring blood sugar. One popular "minimally invasive" glucometer requires smaller sample volumes of blood than the traditional method and therefore can take samples from the forearm where nerves are not as close together as they are on the fingertip [10]. This monitor operates within the standards set by the FDA (United States Food and Drug Administration) but is not as accurate as a traditional glucometer. Additionally, the FDA has recently approved two "non-invasive" glucometers for continuous blood sugar monitoring over twelve hours. One of these monitors, the GlucoWatch Biographer, is worn on the wrist and

passes a low electrical current through the skin. The current draws glucose-containing fluid through the skin by a process called reverse iontophoresis. This fluid is then analyzed by the GlucoWatch for its glucose content. The device is not the non-invasive monitor diabetics have longed for because it lags behind traditional finger stick methods by approximately eighteen minutes, causes skin irritation in up to 50% of its users, and requires daily calibration by invasive glucometers [11]. The GlucoWatch is not recommended as a replacement for the traditional measurement, only a supplement between normal testing [12]. Annual sales of glucometers total \$2 billion, and yet there is no monitor on the market that fully meets consumer's needs for painless, accurate measurement [13].

Recent research performed in the Microwave Applied Metrology Lab (MAML) at Baylor University suggests that there may be a painless, non-invasive method for determining *in vivo* glucose concentration. Through microwave spectral analysis of blood, it may be possible to determine a diabetic's blood sugar concentration as a function of the electrical characteristics of his tissues, such as the electrical permittivity. Therefore, it is important to know the electrical properties of human blood, skin, fat, muscle, and bone which will be outlined in Chapter Five.

CHAPTER THREE

Microwave Properties and Measurement

The observable electromagnetic frequencies range from 0 to 10^{23} Hz, representing a span from DC, a signal that does not oscillate, through audible, radio, infrared, visible light, ultraviolet light, x-ray, gamma ray, and cosmic ray frequencies (see Fig. 2). The term microwave is typically used to describe the frequency range from 100 MHz to 100 GHz, which falls within the radio wave portion of the spectrum.

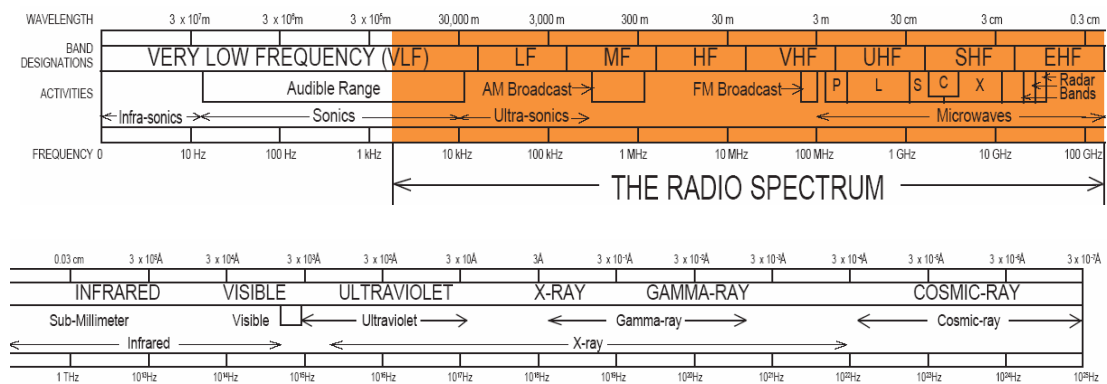


Fig. 2: The electromagnetic spectrum [14]

The building blocks of all matter are electrically charged protons and electrons as well as non-charged neutrons. Everything in the known universe is comprised of mixed arrangements of these fundamental electrical particles. As a result, all substances possess electrical properties. Knowledge of these properties can be utilized to understand how a given material will react under specific circumstances. The property monitored by microwave sensors is permittivity.

Permittivity, ϵ , is a measure of how much electrical energy a material stores and dissipates when it is in an electric field. When an electric field is present, a material will adjust the positioning of its ions or electrons to receive energy from the field. This electrical displacement, D , (also known as electric flux density) divided by the strength of the field causing the displacement, E , is the permittivity of an object measured in farads per meter (F/m). Relative permittivity, ϵ_r , is a unitless ratio of the permittivity of an object to the permittivity of free space (vacuum), ϵ_0 , which is 8.85×10^{-12} F/m [15]. A material's permittivity varies with frequency but is often represented by its value at DC.

Permittivity can be a complex number, often written as:

$$\epsilon = \epsilon' - j\epsilon'' \quad (1)$$

The imaginary part of permittivity, ϵ'' , is the loss factor, a measure of an electric field's energy loss when passing through a material. The real part of permittivity, ϵ' , is the dielectric constant, a measure of a material's energy storage when an electric field is present. It naturally follows that the real part of the *relative* permittivity is the *relative* dielectric constant. As can be inferred from the value of ϵ_0 above, relative dielectric constant values are easier numbers to work with than actual dielectric constant values. Because of this, the majority of microwave researchers use *relative dielectric constant* values, despite typically referring to them simply as the *dielectric constant*. This convention is adopted in this study as well.

There are several ways to measure a material's permittivity; three will be presented in this chapter. One method used in the MAML utilizes a rectangular waveguide. A rectangular waveguide is a metal box, open at one or both ends, with known dimensions, a and b (see Fig. 3). It is possible to pass a range of frequencies

through a filled waveguide and locate material-dependant cutoff frequencies, f_c , of each propagating mode. Further background on measuring permittivity at f_c is found in [2].

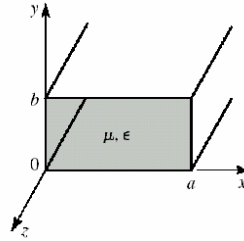


Fig. 3: Diagram of a rectangular waveguide [16]

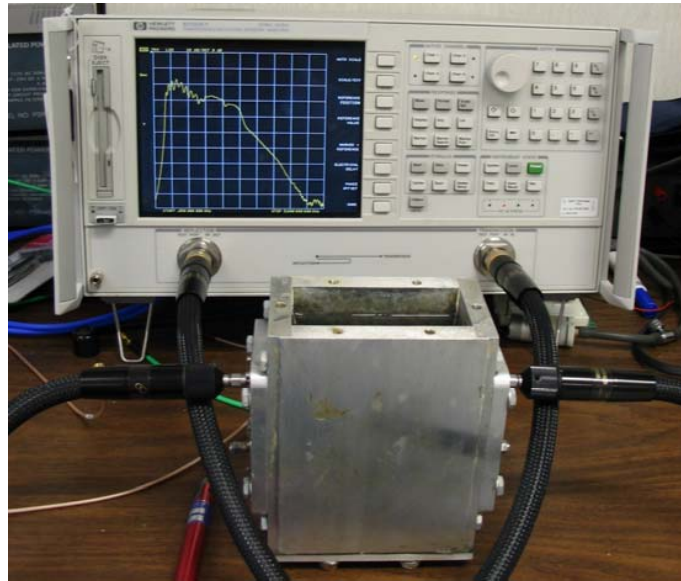


Fig. 4: Hewlett Packard 8720ET Vector Network Analyzer connected to a rectangular waveguide

In Figure 4 a typical rectangular waveguide setup is pictured. The waveguide is connected to the transmission and reflection ports of a vector network analyzer (VNA), a tool which determines the S-parameters of a microwave circuit over a range of frequencies. The VNA passes a swept frequency signal through its reflection port into an antenna in the waveguide. The antenna converts the signal into an electromagnetic wave. When f_c of the TE_{10} mode is reached, the wave begins to propagate through the

waveguide, where it is detected by a second antenna and returned to the VNA through its transmission port (see Fig. 5). The VNA graphically reports the waveguide output versus frequency, and the cutoff frequencies are determined from visual inspection of the data.

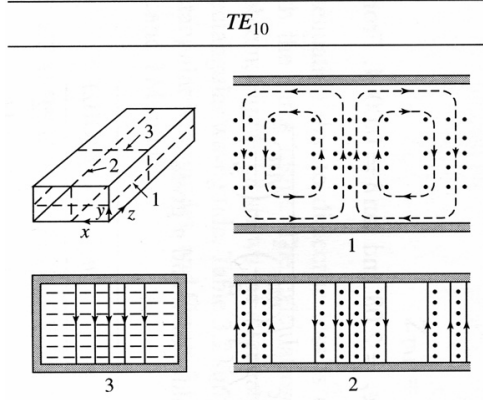


Fig. 5: The field lines for a TE_{10} wave propagating inside a waveguide [16]

This method of measuring permittivity, while straightforward, has limitations. Often, due to losses in the material, a particular mode's cutoff frequency is hard to determine, so a best guess must be made. Additionally, the method in [2] only finds the permittivity of a material at its cutoff frequencies. This limitation presents a problem, since permittivity is a frequency dependant property. Mathematical models do exist that use the entire spectrum to determine permittivity over a range of frequencies. However, these models can be prohibitively complex and are better handled by computers running advanced analysis programs.

Another useful tool for measuring electrical permittivity is an open-ended coaxial probe (see Fig. 6). The probe is nothing more than a center conductor surrounded by a dielectric material and an outer conductor, much like an open-ended coaxial line. If the probe were an actual coaxial cable, the cable's dielectric could be damaged easily and its response changed. To prevent this, the probe's dielectric material is made of a stable,

non-reactive substance (i.e., glass) that allows the probe to be used in caustic environments over a range of temperatures.

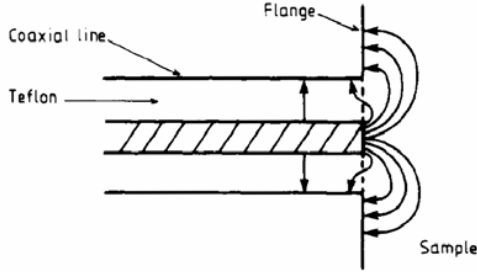


Fig. 6: Field lines for an open-ended coaxial probe [17]

The probe is easy to use. When a signal is transmitted to the probe, the sample is seen as a load. Energy is passed into the sample, where it displaces the ions and charge carriers in the sample. This energy change causes a reflection, $\Gamma(\omega, \epsilon)$, that is measured by the VNA. $\Gamma(\omega, \epsilon)$ is a complex value, dependant on the permittivity of the sample and the angular frequency at which the reflection was measured. With $\Gamma(\omega, \epsilon)$ known, the characteristic admittance of the load may be calculated by:

$$Y_L(\omega, \epsilon) = Y_o \frac{1 - \Gamma(\omega, \epsilon)}{1 + \Gamma(\omega, \epsilon)} \quad (2)$$

where Y_o is the characteristic admittance of the probe. With $Y_L(\omega, \epsilon)$ calculated, permittivity may be found from the equation:

$$Y_L(\omega, \epsilon) = j\omega C_1 + i\omega C_0 \epsilon + jA\omega^3 \epsilon^2 + B\omega^4 \epsilon^{2.5} \quad (3)$$

by using an appropriate iterative process [18]. This is most easily done using a computer.

In the MAML, the primary method of measuring permittivity is with an Agilent Dielectric Probe Kit (Agilent Technologies, Palo Alto, CA) (see Fig. 7). The kit includes an open-ended coaxial probe, calibrating standards, and a computer interface. To obtain

accurate permittivity data, a calibrated probe needs to be in full contact with the sample; no air may exist between the sample and the probe. Once the measurement is triggered, Equation (2) and Equation (3) are used to calculate permittivity.

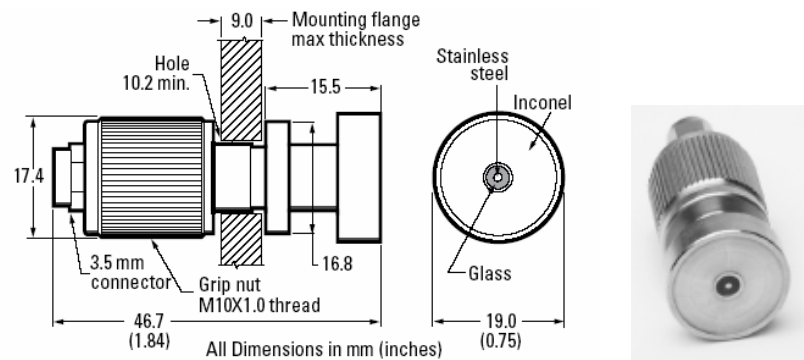


Fig. 7: The Agilent High Temperature Dielectric Probe [19]

Although their design is not as standardized as waveguides and coaxial probes, resonant sensors are another type of tool for measuring a material's permittivity. A resonant sensor is simply a sensor whose S-parameters change in a measurable way as the permittivity of the material being measured changes. Specifically, a resonant sensor has a peak or valley in its frequency response that occurs at a resonant frequency. For some resonant sensor structures, there are detailed mathematical models to determine an object's permittivity at the resonant frequency. However, there are countless resonant microwave structures so complex that mathematical models are nearly impossible to devise. One way to extract permittivity information from these complex sensors is by comparing their output to the output of a simulated sensor. Using Programs like CST Microwave Studio (CST, ver. 5.1.1, January 17, 2005, Germany) repetitively to simulate resonant structures with various loads, it possible to build a lookup table of permittivity vs. resonant frequency.

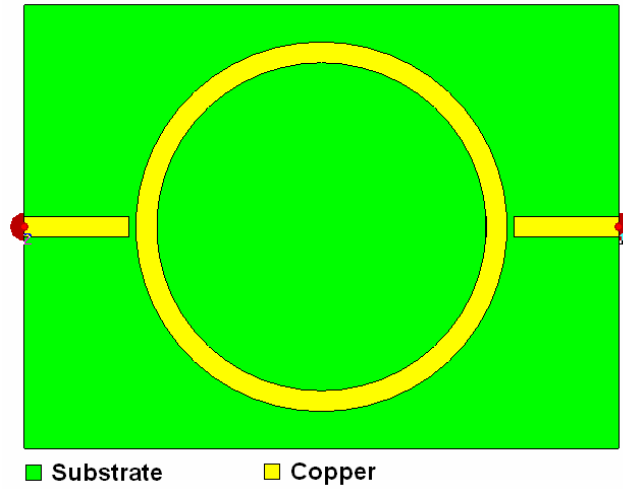


Fig. 8: Ring resonator circuit

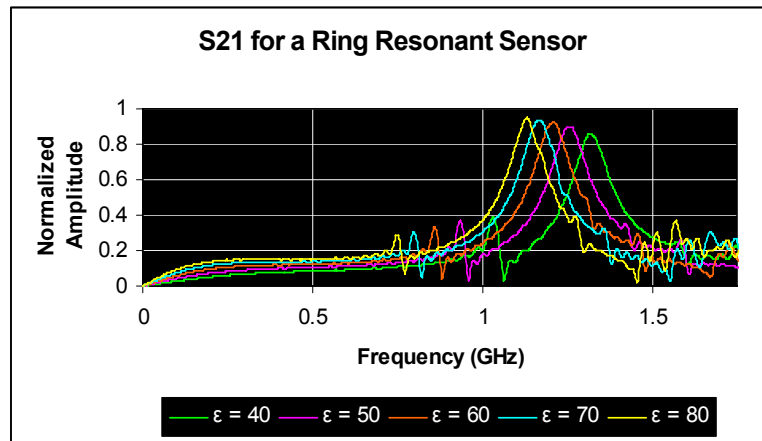


Fig. 9: Output plot for a ring resonator circuit

An example of a ring-resonant sensor and its response are presented in Figure 8 and Figure 9. As the permittivity of the material on top of the ring increases, the ring's resonant frequency, where the peak occurs, decreases. The ring's resonant behavior is easily explained. When a signal enters the ring from the coupling gap on the left, the energy coupled into the ring splits equally over the top and bottom of the ring. This produces a standing wave such that when the ring is in resonance, the maxima of the

wave occur at the coupling gaps and the nulls are at the top and bottom of the ring [20].

The equation:

$$2\pi r = \lambda_g \quad (4)$$

where r is the ring's radius, may be used to determine the wavelength that will produce the ring's first-mode resonance. The resonant frequency of the ring occurs when:

$$f = \frac{c}{\lambda_g \sqrt{\epsilon_{eff}}} \quad (5)$$

This is simplified with Equation (4) to yield:

$$f = \frac{c}{2\pi r \sqrt{\epsilon_{eff}}} \quad (6)$$

where c is the speed of light and ϵ_{eff} is the effective permittivity. The ring resonator is only able to determine electrical permittivity at its resonant frequencies.

These methods are just three of the numerous ways of measuring an object's permittivity. All methods have advantages and disadvantages, such as ease of design, stability, and size. In Chapter Six, these three methods will be given specific consideration in the development of a non-invasive biological sensor.

CHAPTER FOUR

Biology and Microwaves

The human body is constantly exposed to high frequency electromagnetic energy. Cell phones, wireless routers, television stations, and satellites are just a few of the microwave sources whose signals constantly bombard people who live in most urban areas [14]. Microwave energy and biology have had a long history together, and concerns about the physiological effects of microwaves have been around since the beginning. In response to these concerns, standards of microwave exposure were developed by researchers searching for a clearer picture of the physiological effects of microwaves. Over time, these standards were revised and updated to the standards in use today. While questions remain about electromagnetic energy's effect on human tissues, the field strengths of the examples above are so low that there is little concern regarding harmful biological effects. In fact, all these signals are well within the safe exposure standards set by the Institute of Electrical and Electronics Engineers (IEEE). These standards (see Table 1) specify an acceptable exposure of less than 1.6 W/kg of electromagnetic energy for any part of the body [21].

Table 1: IEEE recommendations for Specific Absorption Rates (SAR) of electromagnetic energy [21]

Exposure Characteristics	Frequency Range	Whole-Body (W/kg)	Partial-Body (W/kg)	Hands, Wrists, Feet, and Ankles (W/kg)
Occupational Exposure	100 kHz - 6 GHz	0.4	8	20
General Public Exposure	100 kHz - 6 GHz	0.08	1.6	4

During the early to mid-twentieth century, researchers illustrated that diathermy, the process of heating tissue with electromagnetic energy, was an effective method for treating tumors [22]. Diathermy relies on microwaves' ability to heat a localized region in the body without greatly affecting tissues between the region and the microwave source. Diathermy, also called hyperthermia, may be used to kill tumors, improve drug delivery, and break-up blood clots.

As researchers worked to improve the therapeutic use of diathermy, it became increasingly necessary to understand the dielectric properties of individual biological tissues. H. P. Schwan was a primary researcher involved in developing this understanding [23]. His work is still widely cited today, and his understanding of biological permittivities helped pave the way for more advanced microwave biomedical fields, such as microwave thermography.

Microwave thermography is the process of measuring temperature inside the body as a function of passive thermal radiation given off by the body [24]. Thermography may be used non-invasively to measure numerous physiological parameters, including skin thickness, presence of a tumor, inflammation, intensity of pain, tissue densities, blood flow, and severity of burns [25-27]. Infrared radiation is actually the strongest type of thermal radiation, but because of high attenuation of infrared signals in tissue, microwave thermography is preferred for measuring temperatures inside the body.

Of course, not all microwave devices that measure physiological parameters rely on passive radiation. Microwave imaging and tomography use the transmission and reflection of microwaves incident on a body to image structures in the body, similar to CAT scans and MRI's. Microwaves offer a way to see inside the body without

application of the ionizing radiation used in x-rays. Unfortunately, microwave tomography has to overcome many hurdles before it is commercially viable, including wavelength resolution issues, scattering problems, diffraction, object size and geometry, and solution speed [28].

One application of microwave imaging does show promise. Biomedical researchers have developed systems capable of locating and imaging breast tumors in women. Even with the aforementioned limitations of microwave imaging, this application is possible because the electrical permittivity of malignant breast tissue is vastly different from that of the surrounding tissue [29]. While microwave tomography seemingly has nothing to do with designing a microwave glucometer, researchers working on tomography and other biomedical applications have developed a host of microwave sensors whose properties should be given consideration during the development of this sensor.

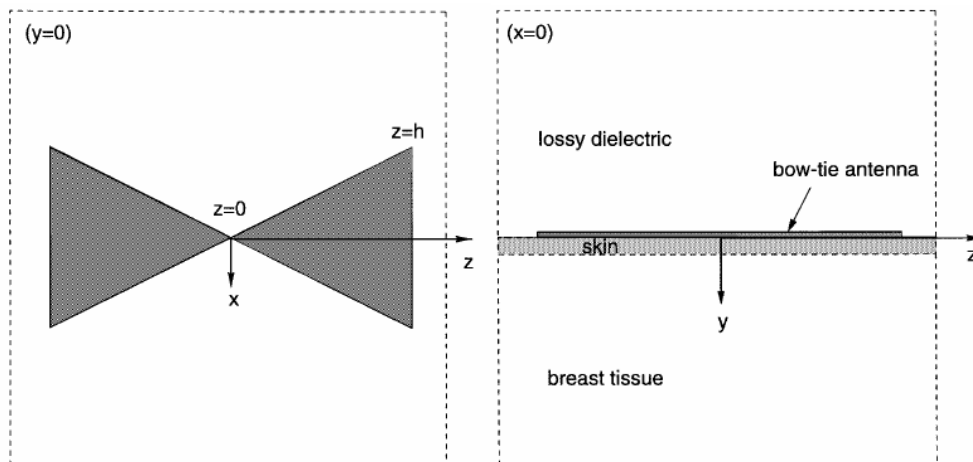


Fig. 10: Bowtie antenna developed for microwave mammography

A bowtie antenna has been developed to couple energy into the breast and measure the backscatter from tumors and dense tissues (see Fig. 10) [30]. The

advantages of the antenna are its ability to be inexpensively manufactured, its planar structure, and its wide-band response. These properties of bowtie antennas make them well suited for a variety of biological measurements, not just microwave mammography [31].

A variation of the typical bowtie antenna, a bowtie-slot antenna, has been used in microwave plethysmography. Plethysmography is the practice of measuring certain physiological parameters to estimate the size of an organ. Gentili *et al.* used the antenna in Figure 11 to non-invasively measure heart and lung volumes [32]. As with microwave mammography, the bowtie structure was selected because of its wide bandwidth, cost effectiveness, and planar structure. Additionally, the bowtie configuration can be manufactured on thin, flexible circuit material so that it may closely adhere to the skin without interference by air.

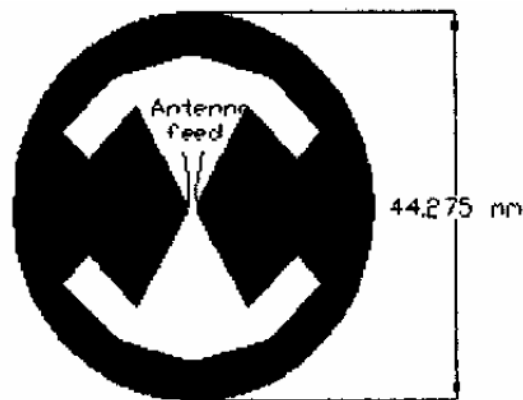


Fig. 11: Bowtie-slot antenna used in microwave plethysmography

There are many varied applications of microwave technologies in medicine. The examples provided in this chapter are in no way comprehensive, and yet there is much more medical frontier to explore. As was mentioned in Chapter Two, there is no suitable

non-invasive device for measuring blood glucose concentration. Using the principles from Chapter Three, as well some of the microwave techniques currently used in medicine, it seems highly likely that a microwave solution exists to this problem. Before an attempt at solving this problem may be made, it is first necessary to have an understanding of how biological specimens behave in the presence of microwaves, which will be explained in Chapter Five.

CHAPTER FIVE

Microwave Properties of Biological Materials

In order to predict the effects of microwave radiation on the body, a full understanding of the dielectric properties of tissue is necessary. This understanding is also needed to aid in the continued development of microwave-based biomedical devices [33, 34, 35].

The main component of biological materials is water, a highly polar molecule that one would expect to be the primary contributor to permittivity [34]. However, biological materials do not behave as simple mixtures of components but have a complicated electrical response. Considerable effort has been invested into determining not just permittivity values for various tissue types, but also models to explain tissue's somewhat surprising electrical behavior. Specifically, biological substances have exceptionally high dielectric constants at sub-microwave frequencies. This phenomenon is seen in Figure 12, a generalized plot of biological tissue permittivity from near-DC to 100 GHz. The generalized curve has four distinct regions of decreasing dielectric constant, called α -dispersion, β -dispersion, δ -dispersion, and γ -dispersion.

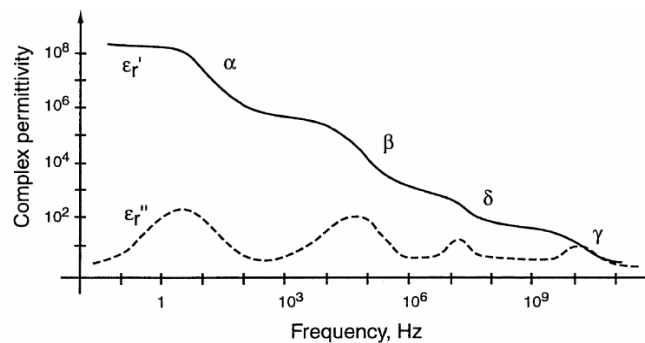


Fig. 12: Idealized dispersion regions for tissue [36]

While the effects of α -dispersion are negligible at microwave frequencies, this region of the curve is where the dielectric constant looks the least like water, and thus it cannot be ignored. The unusually high dielectric constant of this region is due to a charge buildup that results from interfacial polarizations [33]. These polarizations, called Maxwell-Wagner polarizations, occur at the junction of two different dielectrics and form a resistive barrier. This situation occurs at the boundary of cells – little packets of fluid and organelles held closely together to form tissues. The outer layer of a cell is a highly capacitive membrane that is 3 nm thick [36]. An electrolyte, consisting of water and ions, fills the space between cells as well as much of the volume within cells. Maxwell-Wagner polarizations occur where the highly conductive electrolyte meets the highly capacitive cell membrane.

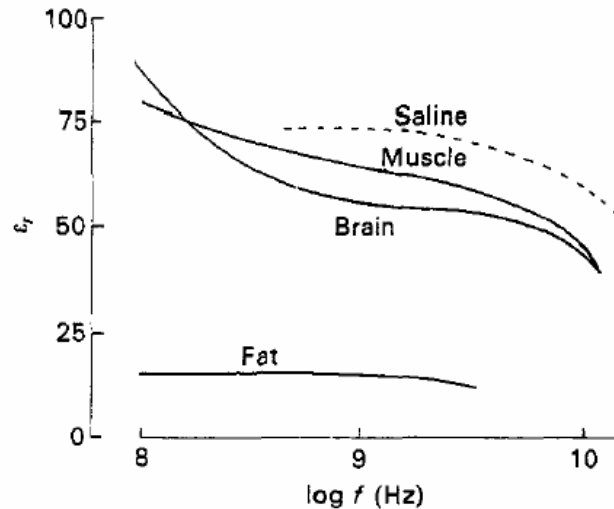


Fig. 13: Dielectric properties of body tissues [33]

As frequency is increased past approximately 1 kHz, the capacitive membrane begins to resemble a short, causing β -dispersion [33]. With cell membranes acting as shorts, the permittivity is based increasingly on the electrolyte; this is why biological

permittivities resemble the main electrolyte component, water. Membrane shorting causes tissues to seem more, but not completely, homogeneous. In Figure 13, the dielectric constant of some tissues compared to electrolyte solution (saline) are presented. Because the curves are not identical, this plot illustrates that the permittivities of biological materials show limited influence of the non-polar membrane and biochemicals between 100MHz and 1GHz.

The δ -dispersion is actually a subset of β -dispersion. At frequencies slightly higher than the β -dispersion of cell membranes, protein-bound water exhibits a molecular relaxation [36]. Bound water accounts for approximately 10% of water in tissues. Water is considered “bound” when the location of the water molecule and its interaction with proteins prevents the water’s full rotation in an electric field [37]. This causes the relaxation frequency of bound water to be 50 to 100 times lower than normal water’s molecular relaxation frequency, which occurs around 10 GHz. This relaxation of non-bound water is the cause of γ -dispersion.

With the general dielectric properties of biological materials known, further attention must be paid to the specific tissues a glucose sensor would encounter. These tissues include skin, fat, muscle, bone, and most importantly blood. The relative dielectric constants of these tissues have been extensively researched, and various mathematical models have been developed [38]. One such model is the Cole-Cole model for multiple dispersions, which is expressed as:

$$\hat{\epsilon}(\omega) = \epsilon_{\infty} + \sum_n \frac{\Delta\epsilon_n}{1 + (j\omega\tau_n)^{(1-\alpha_n)}} + \frac{\sigma_i}{j\omega\epsilon_0} \quad (7)$$

Equation (7) was used to produce the plots in Figure 14 and Figure 15, which illustrate the relative dielectric constants of the above tissues. In Figure 15, the frequency is

limited between 50 MHz and 2 GHz. This span represents the operating range of the glucose sensor that will be discussed in more detail in Chapter Six.

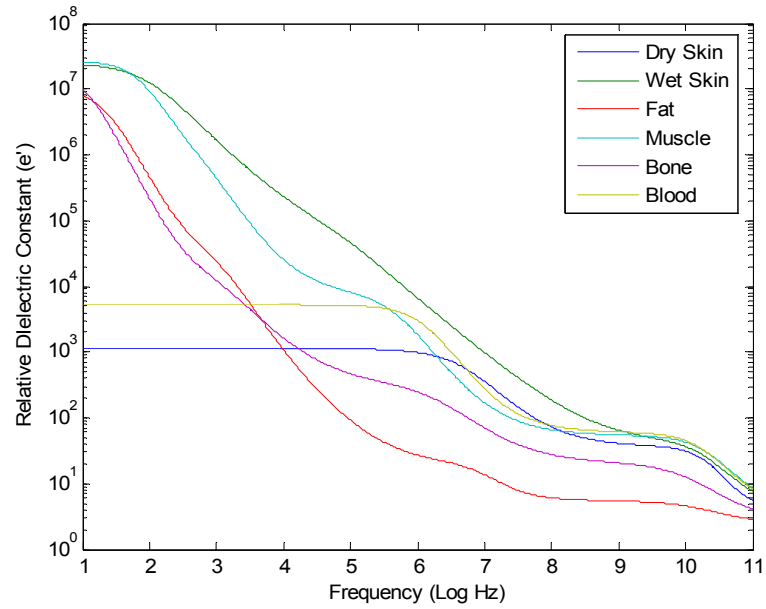


Fig. 14: Relative dielectric constant of certain tissues from 10 Hz to 100 GHz, created from Equation (7)

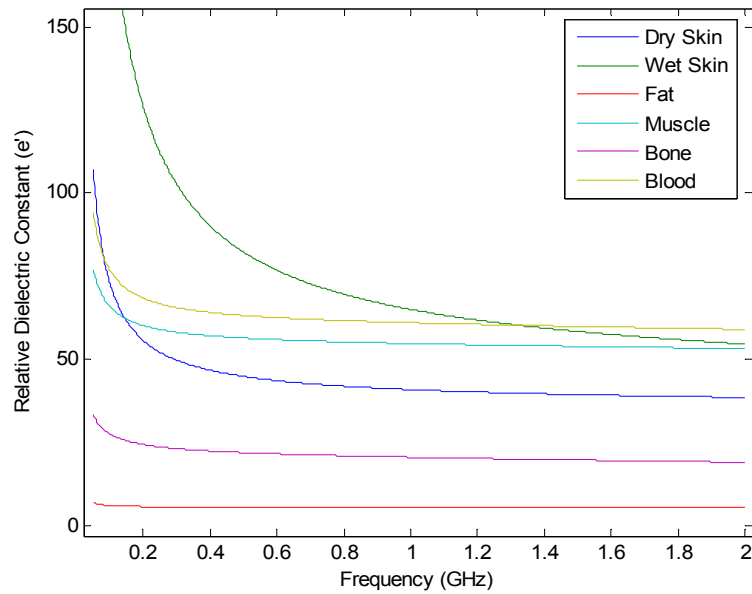


Fig. 15: Relative dielectric constant of certain tissues from 50 MHz to 2 GHz, created from Equation (11)

As was stated earlier, tissues exposed to radiation in the microwave frequency range exhibit properties strongly dependant on the behavior of water. It is commonly held that percentage of water content is related to dielectric constant [33, 34, 35, 38]. For example, fat has very little water, whereas it is the main constituent of blood.

Table 2: Parameters of the Cole-Cole model for certain tissues [38]

	Dry Skin	Wet Skin	Fat	Muscle	Bone	Blood
ϵ_{∞}	4	4	2.5	4	2.5	4
$\Delta\epsilon_1$	32	39	3	50	18	56
τ_1	7.23E-12	7.96E-12	7.96E-12	7.23E-12	1.33E-11	8.38E-12
α_1	0	0.1	0.2	0.1	0.22	0.1
$\Delta\epsilon_2$	1100	280	15	7000	300	5200
τ_2	3.25E-8	79.58E-9	1.59E-8	3.54E-7	7.96E-8	1.33E-7
α_2	0.2	0	0.1	0.1	0.25	0.1
$\Delta\epsilon_3$	0	3E4	3.3E4	1.2E6	2E4	0
τ_3		1.59E-6	1.60E-4	3.18E-04	2E-04	
α_3		0.16	0.05	0.1	0.2	
$\Delta\epsilon_4$	0	2.5E7	1.0E7	2.5E7	2.0 E7	0
τ_4		.0016	0.008	0.002	0.016	
α_4		0.2	0.01	0	0	
σ	2E-4	4E-4	0.01	0.2	0.07	0.7

The information in Figure 15 suggests that the placement for the glucose sensor should be an area with as little fat content as possible. A design goal of the sensor is to maximize the amount of energy coupled into and back out of tissues. To do this, transmission between tissue layers must be maximized. A signal passing between two mediums of different dielectric constant is governed by the transmission coefficient, which is expressed as:

$$T = \frac{2\eta_2}{\eta_2 + \eta_1} \quad (8)$$

where η_i is the intrinsic impedance of a material, defined as:

$$\eta = \sqrt{\frac{\mu}{\varepsilon}} \quad (9)$$

where μ is a material's magnetic permeability [15, 16]. For biological tissues, magnetic permeability is approximately equal to the magnetic permeability of free space [33].

Substituting Equation (9) into Equation (8), yields:

$$T = \frac{2\sqrt{1/\varepsilon_2}}{\sqrt{1/\varepsilon_2} + \sqrt{1/\varepsilon_1}} = \frac{2\sqrt{\varepsilon_1}}{\sqrt{\varepsilon_2} + \sqrt{\varepsilon_1}} \quad (10)$$

This means that at 1 GHz, a wave traveling between fat and skin has approximately 50% transmission, whereas a wave traveling between muscle and skin has nearly 93% transmission. Additionally, fat is less vascularized than muscle, so a sensor's electromagnetic fields will come into contact with more blood when placed over muscle as opposed to fat. If more blood is measured, the blood glucose sensor should perform better.

Ultimately, the sensor needs to be capable of detecting changes in the permittivity of blood. Blood is not a homogeneous liquid, but is actually a suspension of cells, proteins, hormones, glucose, and other particles in water. Blood's permittivity is influenced by each of its constituents. Fortunately, microwave sensors are capable of measuring one specific parameter in an environment in which several parameters may change [39]. Therefore, specific attention needs to be paid to glucose's impact on blood's dielectric properties.

In [40], Hayashi *et al.* determined that there is a correlation between D-glucose concentration and the dielectric constant of a suspension of red blood cells, the main constituent of blood (see Fig. 16) [40]. Additionally, they observed no effect on the

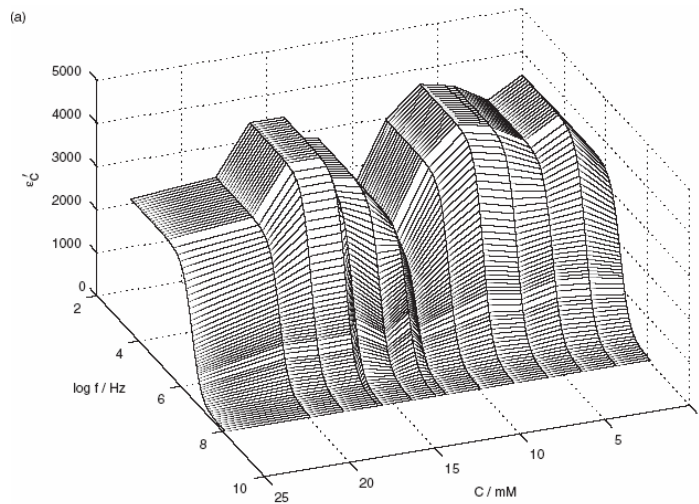


Fig. 16: Influence of D-glucose on dielectric constant of erythrocyte suspension [40]

dielectric constant with changing L-glucose concentration, which was expected since L-glucose is a biologically inactive molecule. The authors pointed out that the effect of glucose on dielectric constant was unexpected because the dielectric relaxation of glucose is heavily masked by that of water in blood or in an aqueous suspension of cells. Instead, the authors believed they measured changes in the permittivity of the erythrocyte cell membrane that was triggered by changing concentrations of glucose inside the cell. This process is illustrated in Figure 17, where glucose enters a cell, is converted to ATP,

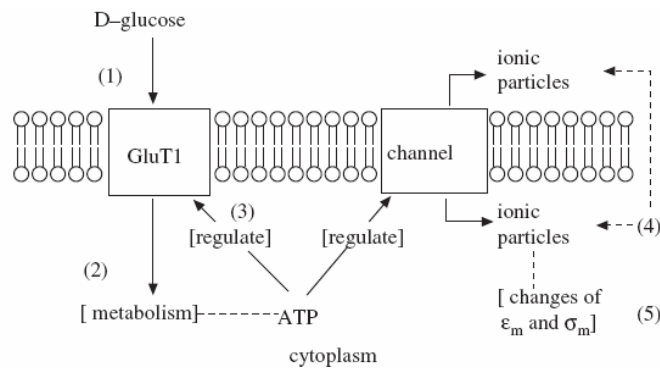


Fig. 17: Suggested mechanism for change in cell membrane permittivity as a function of glucose concentration [40]

which facilitates movement of ions through ion channels in the cell membrane. The net result of this process is a change in the cell membrane's permittivity. While these results bode well for the development of a non-invasive glucometer, measurement of a correlation *in vitro* does not guarantee a correlation *in vivo*.

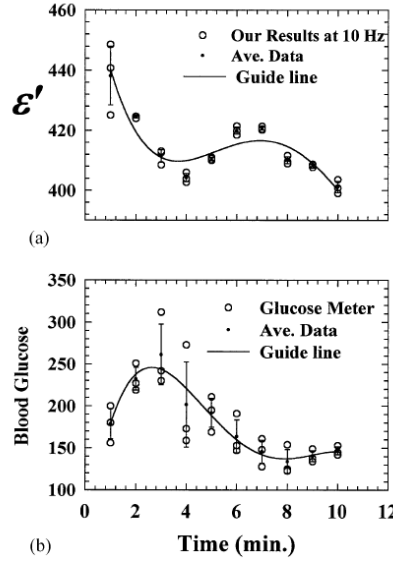


Fig. 18: Plots for (a) dielectric constant at 10 kHz and (b) the hamster's blood glucose concentration after administration of a glucose solution [41]

Park *et al.* attempted to demonstrate a correlation between permittivity and glucose concentration *in vivo* in a hamster [41]. To obtain the measurement, they built a special waveguide that fit over the tail of the hamster. They then fed the hamster samples of glucose in water and measured the dielectric constant of the hamster's tail at 10 kHz. The researchers found that a relationship exists between glucose concentration and dielectric constant of hamster blood at 10 kHz, although the relationship between glucose and dielectric constant is not linear (see Fig. 18).

Caduff *et al.* presented a non-invasive method for determining blood glucose concentration by using impedance, or dielectric spectroscopy [42]. The researchers

swept a frequency from 1 MHz to 200 MHz through a resonant circuit. This frequency range was specifically selected to fall within blood's region of β -dispersion. The resonant circuit was contained in a wristwatch-like case which holds part of the resonant circuit on the user's arm. Since the frequencies of operation are sub-microwave and low-microwave radio frequency signals which penetrate deep into tissues, the characteristic impedance detected by the resonant circuit is a function of not just the tissue touching the sensor, but sub-dermal tissues as well.

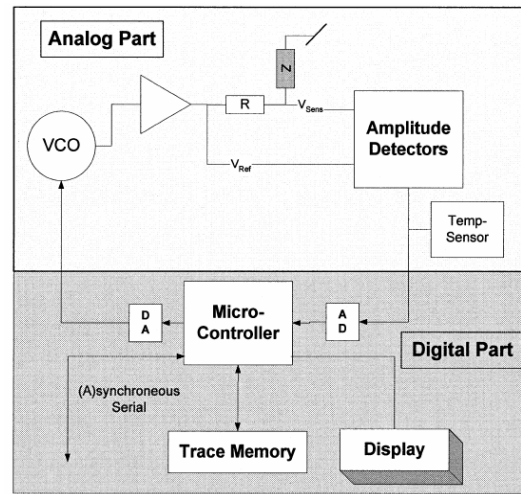


Fig. 19: Layout for non-invasive impedance spectroscopy glucometer [42]

Although Caduff *et al.* provided no information on the configuration of the resonant circuit, schematics in the paper suggest that the sensor most likely relies on reflection, similar to an open-ended coaxial probe (see Fig. 19). Additionally, the authors made their measurements based solely on the reflected resonant frequency. This type of sensor is notoriously difficult to calibrate; therefore, stability may play a role in the accuracy of the meter.

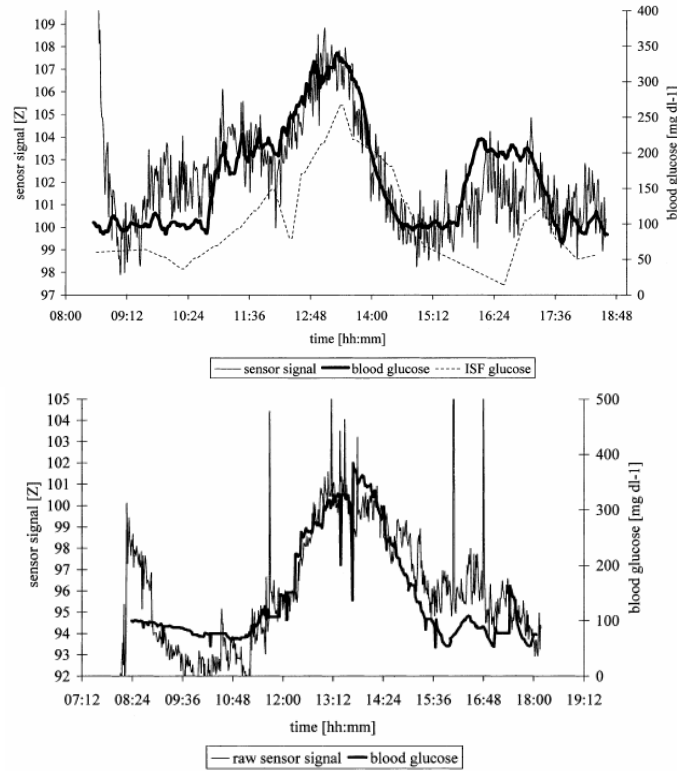


Fig. 20: Glucose profiles measured invasively, and with dielectric spectroscopy [42]

By closely controlling the glucose profiles of human subjects over eight hours, these researchers were able to evaluate the accuracy of their monitor. After an initial settling period of approximately 60 minutes, the data presented illustrated that the devices worked. However, the study mentioned that the method did not work for some people, suggesting that the data presented may not be representative of the performance of the device. Two plots from this study are presented in Figure 20. In the first plot, a sensor signal of 100Ω corresponds to a glucose concentration of 100 mg/dL, but in the second plot, a sensor signal of 100Ω corresponds to a glucose concentration of 300 mg/dL. No explanation is provided regarding this discrepancy. This research, while interesting and novel, seems to have only gone as far as the above referenced article. Extensive searches

on the authors and their work have turned up no recent advances in a non-invasive impedance spectroscopy glucometer.

Unfortunately, no accurate models exist for blood's permittivity as a function of glucose concentration between 50 MHz and 2 GHz. This data is critical for fine-tuning the sensor design. However, given the results of the studies presented above, it seems highly likely that a non-invasive resonant sensor utilizing changes in transmission and reflection may be built and successfully applied to glucose measurement. With information about tissue's electrical properties, typical microwave measurement devices, and current uses of microwaves in biology, sensor design can begin. Chapter Six outlines the antenna design process and gives some specific aspects of the design chosen for fabrication.

CHAPTER SIX

Design of a Microwave Sensor for Electrical Characterization of Biological Materials from 50 MHz to 2 GHz

The task of designing a biological permittivity sensor is not an easy one. Many considerations must be taken into account during sensor design, including sensor type, signal type, frequency range, and sensor size. The design process is iterative, where each prototype is studied for its pros and cons, and then a new prototype is designed accordingly.

Initially, signal type and frequency range had to be selected. Pulse systems are able to operate without interfering with other microwave devices. Therefore, the system was designed for transmission of a pulse, rather than a swept frequency. High bandwidth pulse generators are very expensive, and since this sensor may one day be used in an off-the-shelf glucometer, a low frequency (in terms of microwave frequencies) range was needed. This stipulation is why the frequency range 50 MHz to 2GHz was selected. This span includes the higher frequencies of the β -dispersion (see Fig. 15). Although not visible in Figure 15, the δ -dispersion of the tissues also falls within this frequency range. Penetration depth is a major design parameter to consider. If the fringing fields of the sensor do not extend deep enough into the tissue before returning to the ground plane, the sensor is useless. Since lower frequencies have longer wavelengths than higher ones, lower frequencies penetrate deeper into tissues. Thus, the selected frequency range also benefits the penetration depth of the sensor.

The sensor-type is another important decision. In Chapter Three, three methods of measuring a material's permittivity were presented: waveguide, open-ended coaxial probe, and a resonant sensor. For accurate measurement, a waveguide's dimensions must be precisely known. Since people come in different shapes and sizes, a waveguide is not a viable choice for a glucose sensor. Open-ended coaxial probes are frequently used to measure properties of biological materials [18]. However, the probe is a contact measurement device and must come into close proximity with the material under test (MUT). Since a non-invasive sensor must measure through skin and subcutaneous fat to measure blood, an open-ended coaxial probe is also not the ideal choice. A resonant sensor is a non-contact device able to measure permittivity of arbitrarily shaped objects. Moreover, a planar-resonant sensor may be placed directly on the skin, making it useful in measuring physiological parameters. Waveguides are used to measure signal transmission; open-ended probes are used to measure signal reflection; a resonant sensor can be designed so that the input signal's reflection and transmission both contain useful information about the MUT. For these reasons, a planar resonant sensor was selected as the sensor type for this study.

As discussed in Chapter Five, measurement from a location with minimal fat content and muscles close to the skin will yield the best results. Consequently, there are two obvious anatomical locations where the sensor could be used: on the medial side of the bicep, or on the volar part the wrist. Both of these locations typically have good vasculature and minimal fat. These proposed measurement sites place a size constraint on the sensor.

The development of a microwave sensor is a time consuming process. As stated in Chapter Three, the mathematical models that govern the behavior of microwave structures may be prohibitively complex. Thus, the simplest method to develop a sensor is with microwave modeling software. CST Microwave Studio (MWS) (CST, ver. 5.1.1, January 17, 2005, Germany) accurately predicts the response of a microwave sensor and was chosen for this function in the current study.

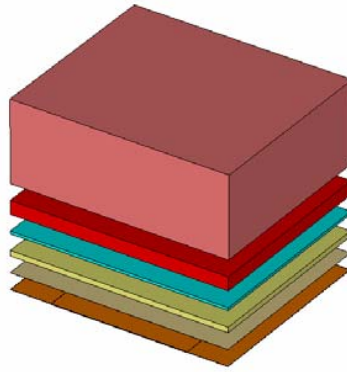


Fig. 21: Layers of the simulated sensor load
From bottom to top: sensor cover film, dry skin, wet skin, fat, blood, and muscle

All the sensor designs described below were developed and tested with MWS. They were tested using the same simulated load, sensor cover film and human tissues, in order to obtain an accurate comparison between sensors as well as a realistic estimation of sensor performance (see Fig. 21). The tissue structure used consisted of a 0.015 mm layer of dry skin, a 0.985 mm layer of wet skin, a 0.5 mm layer of fat, a 2.5 mm layer of blood, and 15.1 mm of muscle. The values in Table 2 were used in the second order Debye equation:

$$\hat{\epsilon}(\omega) = \epsilon_{\infty} + \sum_n \frac{\Delta\epsilon_n}{1 + j\omega\tau_n} \quad (11)$$

to specify permittivity of the tissues [38]. Additionally, simulations were run in which

blood's permittivity was modified to model a parameter shift that may be similar to the one induced by increased glucose concentration (see Fig. 22). The results of the two simulations for each sensor – regular blood and modified blood – were compared, and the metric for a good sensor was one whose $|S_{11}|$ and $|S_{21}|$ plots shifted significantly in frequency, measured at local maxima and minima, with change in load permittivity (see Table 3).

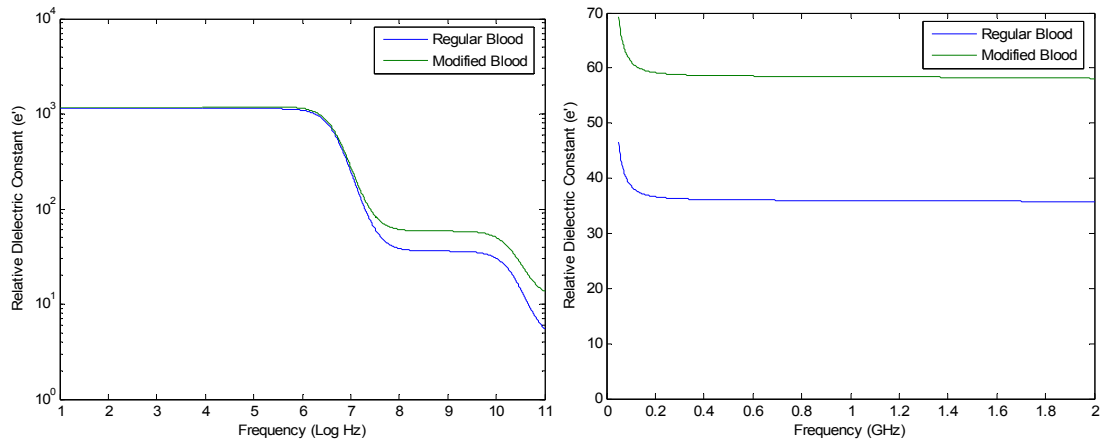


Fig. 22: Second order Debye model of blood and modified blood used in sensor testing

Table 3: Compiled results for sensors designed in this thesis

Resonant Sensor Type	Max shift in $ S_{11} $	Center frequency of $ S_{11} $ shift	Max shift in $ S_{21} $	Center frequency of $ S_{21} $ shift
Microstrip Ring	3 MHz	1.15 GHz	17 MHz	1.6 GHz
Slotline Ring	5 MHz	1.15 GHz	2.2 MHz	1.73 GHz
Microstrip Clover	6 MHz	1.5 GHz	27 MHz	1.6 GHz
Slotline Clover	28 MHz	1.2 GHz	19 MHz	1.15 GHz
Dual Spiral Microstrip	28 MHz	1.6 GHz	27 MHz	1.95 GHz
Single Spiral Microstrip	19 MHz	1.9 GHz	38 MHz	1.72 GHz

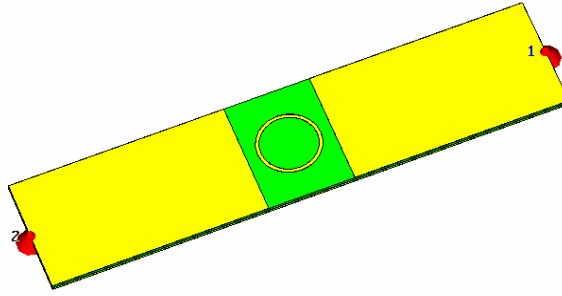


Fig. 23: Microstrip Ring Resonator modeled in CST Microwave Studio

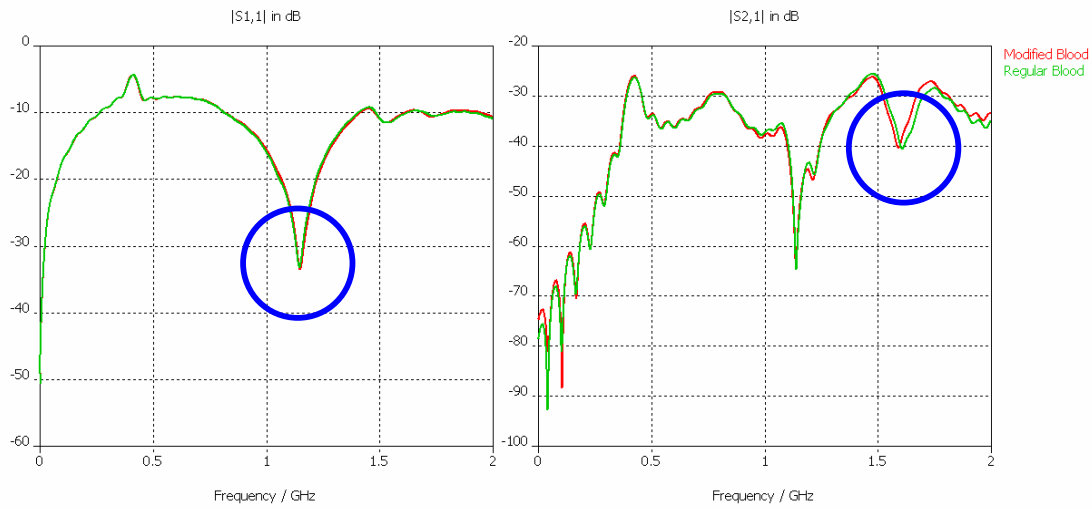


Fig. 24: Response of the Microstrip Ring Resonator

Initially, a microstrip ring resonator was selected because of its predictable nature and ease of design as outlined in Chapter Three (see Fig. 23). The ring was fed by stripline embedded within the substrate. Using Equation (6), and estimating ϵ_{eff} , the ring was designed to resonate near 1 GHz. The ring resonator exhibited good response to changes in load permittivity when in direct contact with a low dielectric. However, when the tissue model was substituted for the load, the ring exhibited little frequency shift between the two models for blood (see Fig. 24). The maximum measurable shifts in the microstrip ring resonator were 3 MHz at 1.15 GHz in the $|S_{11}|$, and 17 MHz at 1.6 GHz

in $|S_{21}|$. While there was no specified frequency shift that this design process was attempting to achieve, 3 MHz shift in the $|S_{11}|$ plot is not adequate.

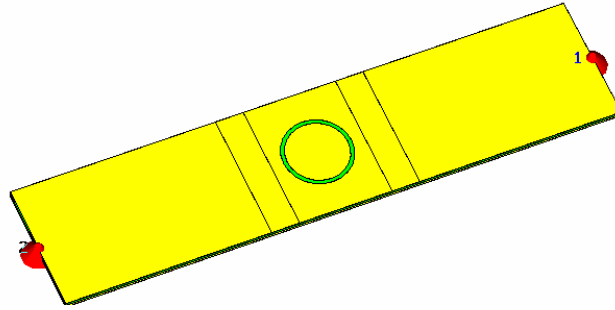


Fig. 25: Slotline Ring Resonator modeled in CST Microwave Studio

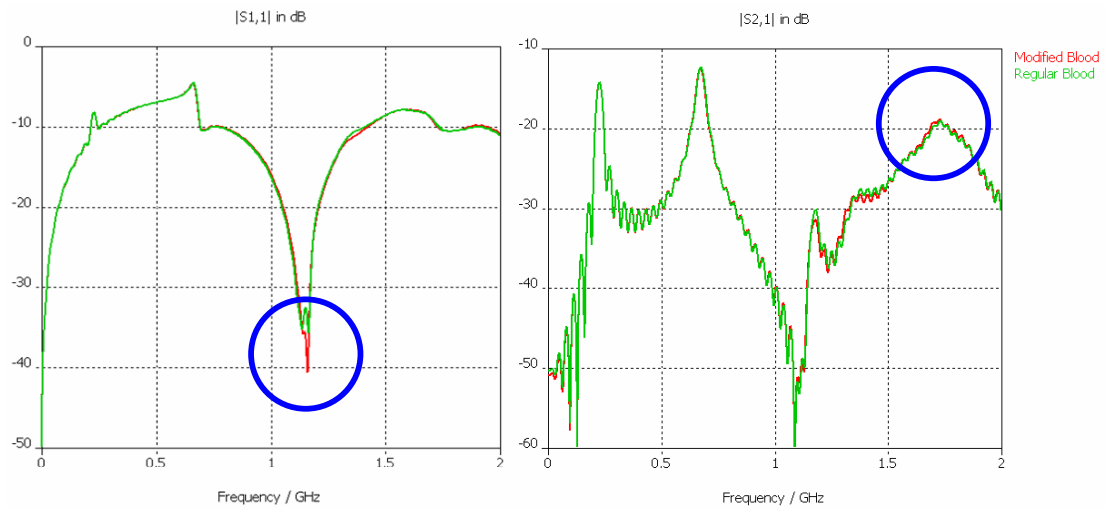


Fig. 26: Response of the Slotline Ring Resonator

A slotline ring resonator structure was then modeled to see if it would have an improved penetration depth over its microstrip equivalent (see Fig. 25). The ring was fed by stripline embedded within the substrate. The $|S_{11}|$ of this sensor showed greater frequency variation (see Fig. 26) with changing permittivity (5 MHz at 1.15 GHz); however, the $|S_{21}|$ of this sensor was considerably worse than the microstrip ring resonator (2.2 MHz at 1.73 GHz).

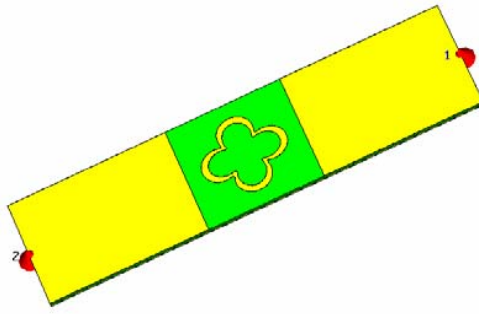


Fig. 27: Microstrip Clover Resonator modeled in CST Microwave Studio

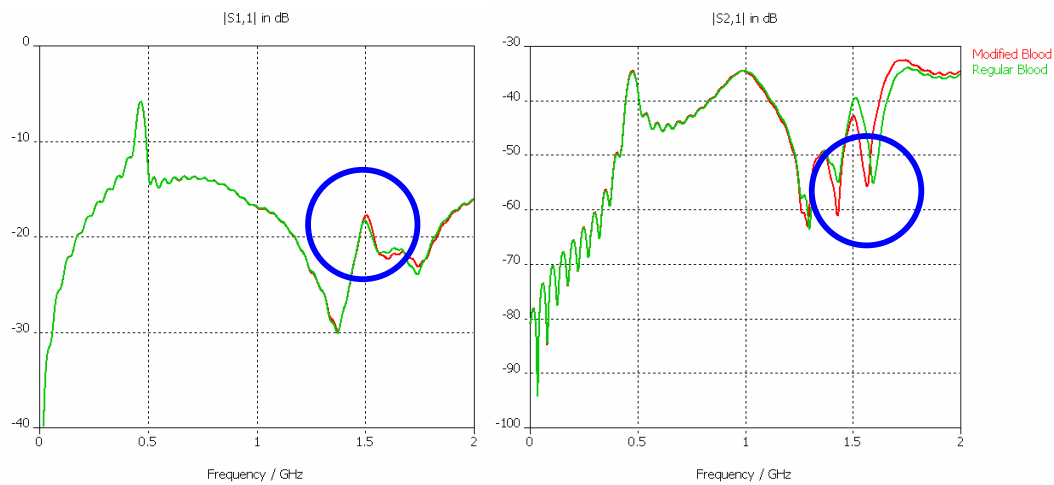


Fig. 28: Response of the Microstrip Clover Resonator

The ring resonator is a very stable structure, therefore it is not ideal for detecting slight changes in permittivity. Instead, a microstrip clover resonator was designed (see Fig. 27). The clover design was based on the ring structure, but the added discontinuities of the petals disrupt the sensor's stability and make it more effective at sensing changes in permittivity. As before, the clover was fed by stripline embedded within the substrate. The clover resonator performed well. The greatest frequency shift in the $|S_{11}|$ was 6 MHz at 1.5 GHz, but more encouraging was the 27 MHz shift in the $|S_{21}|$ at 1.6 GHz. Unfortunately, the $|S_{21}|$ signal was very weak; the majority of it was less than 40 dB (see Fig. 28).

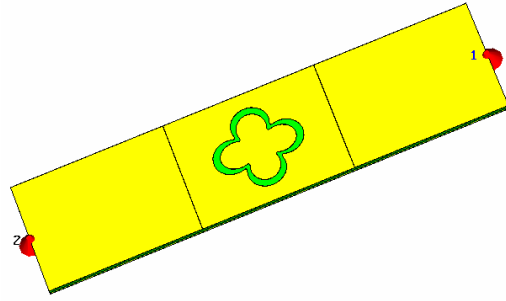


Fig. 29: Slotline Clover Resonator modeled in CST Microwave Studio

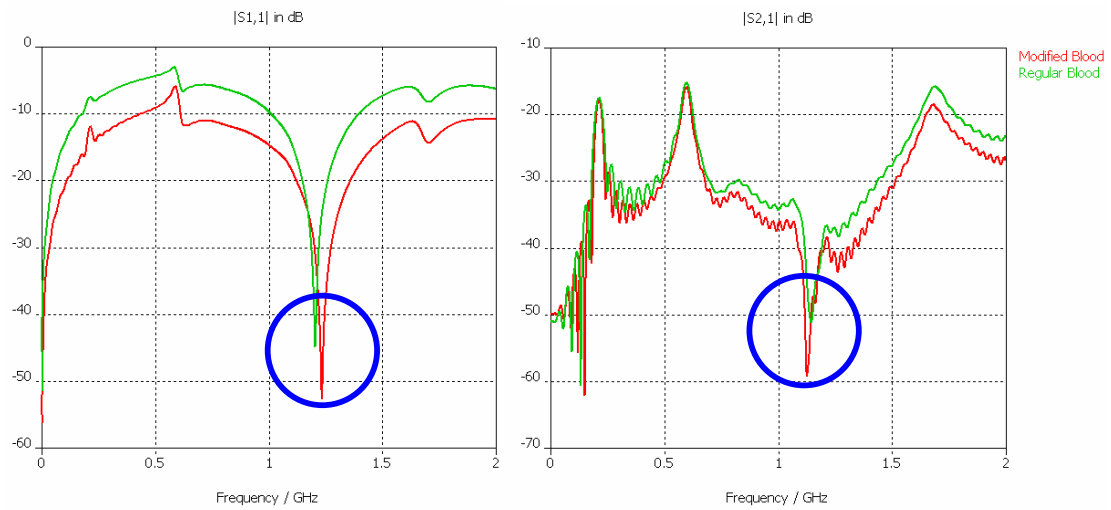


Fig. 30: Response of the Slotline Clover Resonator

To improve on the promising results of the microstrip clover resonator, the next sensor modeled was a slotline clover resonator (see Fig. 29). Again, the sensor was fed by striplines embedded within the substrate. The output of this clover-sensor was much stronger, and it showed good frequency shifts in both reflection and transmission, shifting 28 MHz at 1.2 GHz in the $|S_{11}|$ and 19 MHz at 1.15 GHz in the $|S_{21}|$ (see Fig. 30). This design is considerably improved over the previous three, but the use of slotline is a concern since the slotline gap must be completely filled by the MUT; even a small amount of air between the MUT and the exposed substrate could ruin the measurement.

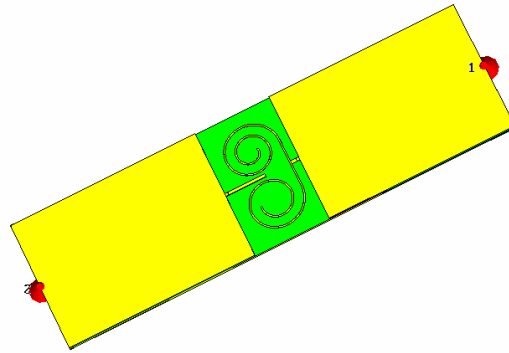


Fig. 31: Dual-Spiral Microstrip Resonator modeled in CST Microwave Studio

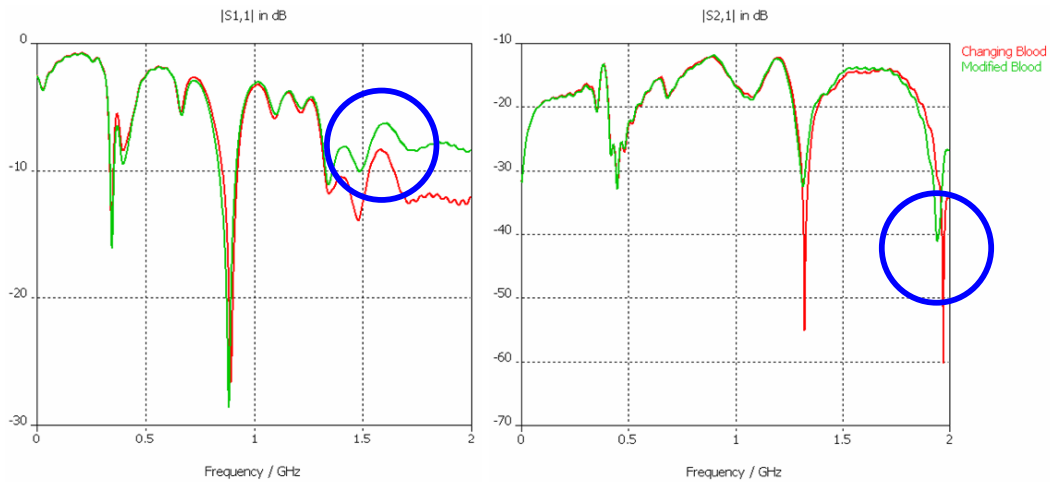


Fig. 32: Response of the Dual-Spiral Microstrip Resonator

As described in Chapter Three, the ring's (and clover's) resonant property results from a standing wave that forms between the ring's input and output. As the permittivity of the sensor load changes, the positions of the peaks and nulls in the standing wave also change. With this in mind, the dual-spiral microstrip sensor was designed. The dual-spiral sensor has two spirals of different lengths, driven by the same source (see Fig. 31). When in operation, standing waves form on the spirals, and energy couples from the spirals into the output trace. As permittivity of the MUT changes, peaks and nulls that form on both traces will move around the spiral. When nulls occur simultaneously at the

output of the spirals, a sharp drop occurs in the $|S_{21}|$. The reverse is true when peaks simultaneously occur at the output. Additionally, the spiral structure was used because, like the clover that worked well before, it is an unstable spin-off of the basic ring design. The dual spiral performed well. The maximum frequency shift in the $|S_{11}|$ was 28 MHz at 1.6 GHz, and the shift in the $|S_{21}|$ was 27 MHz at 1.95 GHz (see Fig. 32).

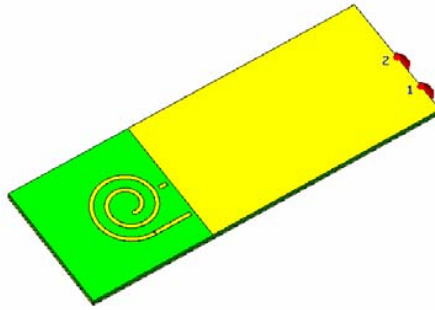


Fig. 33: Single-Spiral Microstrip Resonator modeled in CST Microwave Studio

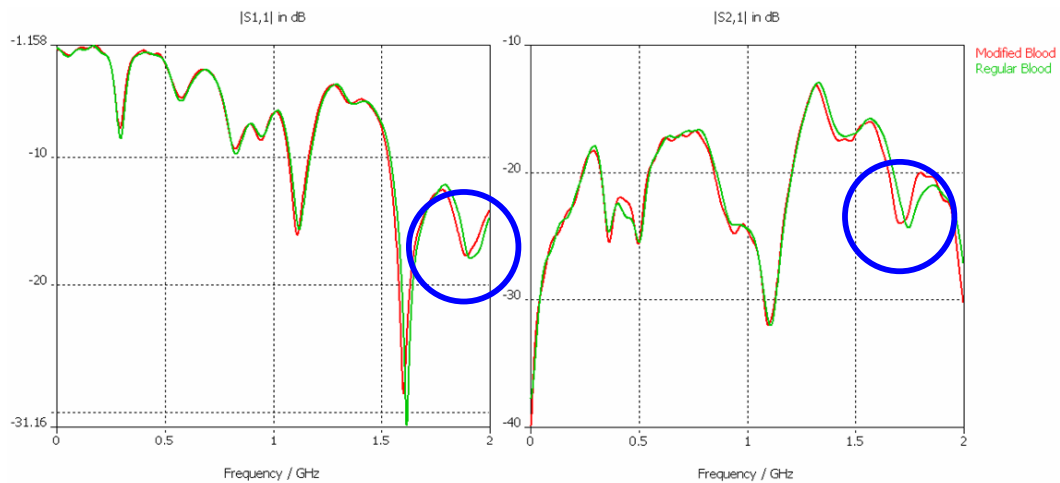


Fig. 34: Response of the Single-Spiral Microstrip Resonator

The well-defined peaks and nulls in the response of the dual-spiral microstrip resonator create a sharp signal that is easily interpreted. However, this clear response comes at the price of a large sensor size. To reduce the size by nearly half, a single-spiral system is employed (see Fig. 33). Similar to the dual-spiral sensor, a standing wave is

present on the single-spiral. On the perimeter of the spiral, an output trace may be placed which essentially samples the spiral signal at that point. As the nulls move around the spiral past the output trace, a dip occurs in the $|S_{21}|$ response (see Fig. 34); this moving null is illustrated in the surface current plot of Figure 35. Although the shift in $|S_{11}|$ is reduced, the frequency response to permittivity changes is still pronounced and even improved in the $|S_{21}|$. The maximum frequency shift of the $|S_{11}|$ is 19 MHz at 1.9 GHz, and the maximum shift of the $|S_{21}|$ is 38 MHz at 1.72 GHz.

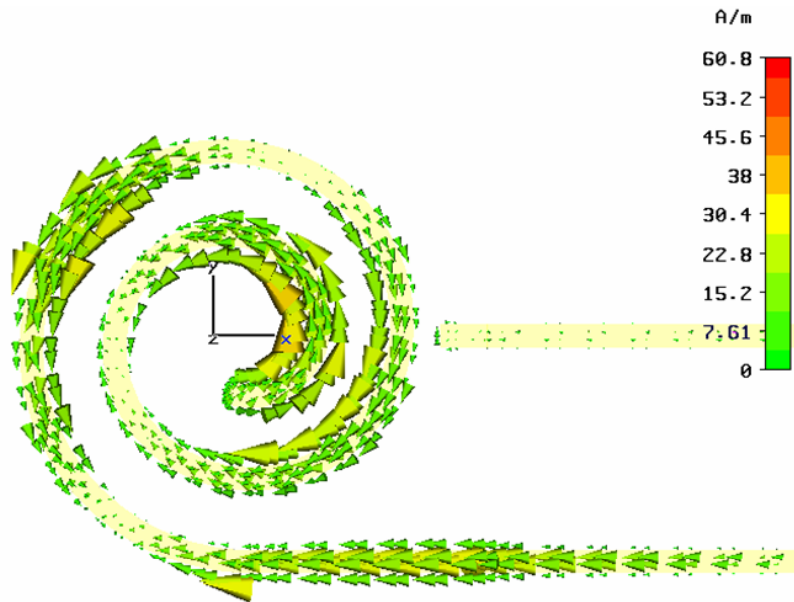


Fig. 35: Surface currents on the single-spiral at 1.5 GHz

Given its frequency response to changes in permittivity as well as its compact size, the single-spiral microstrip resonator was selected for further investigation. In MWS, the sensor accomplishes the stated goal of having multiple features in the $|S_{11}|$ and $|S_{21}|$ that respond to changes in permittivity of the MUT. Chapter Seven illustrates how such a sensor can be used to determine changes in the permittivity of biological material.

CHAPTER SEVEN

Experimental Results from a Single-Spiral Microstrip Resonant Sensor

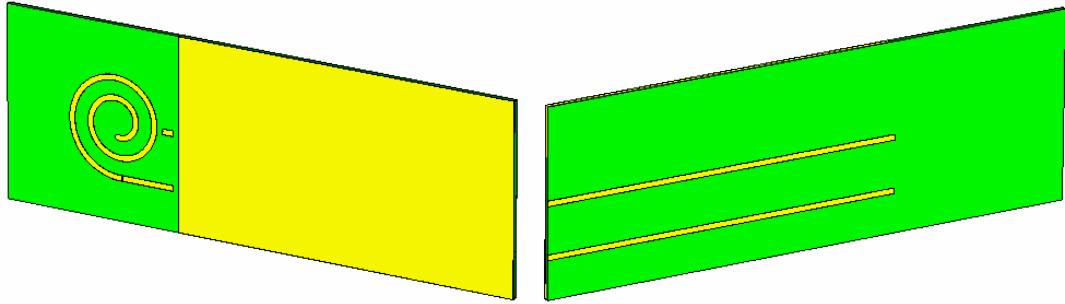


Fig. 36: Front and back view of main layer project board

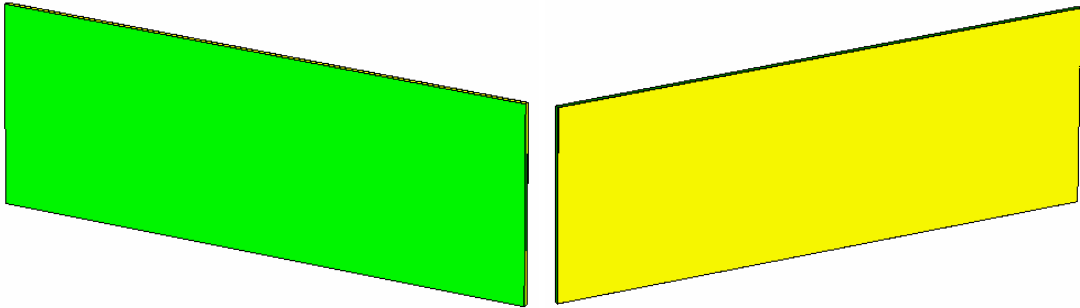


Fig. 37: Front and back view of secondary layer project board

The single-spiral microstrip resonant sensor developed in Chapter Six was fabricated by preparing two boards (see Fig. 36 and Fig. 37). The sensor was etched into double-sided copper-clad project board with FR4 substrate. The copper on the board had a weight of $1\text{-oz}/\text{m}^2$, and the FR4 was $1/32$ in. thick. FR4 has a relative dielectric constant of approximately four at microwave frequencies. Vias were constructed between the striplines and the microstrips that feed the spiral. In addition, a coaxial cable was cut in half. The center conductors were soldered to the striplines, and the outer

conductors were soldered to the ground-plane (see Fig. 38). The two layers of project board were combined using special board adhesive (Rogers 2001-B-200, Chandler, AZ) so that the spiral is in front and the un-etched ground plane is in the rear, leaving the stripline in the middle. Copper tape was applied at the corners and soldered in place, so that the planes above and below the stripline share a common ground. To prevent shorting of the spiral to the ground-plane, a 50 μm -thick layer of cover film was placed over the top surfaces, giving the sensor an orange tint.

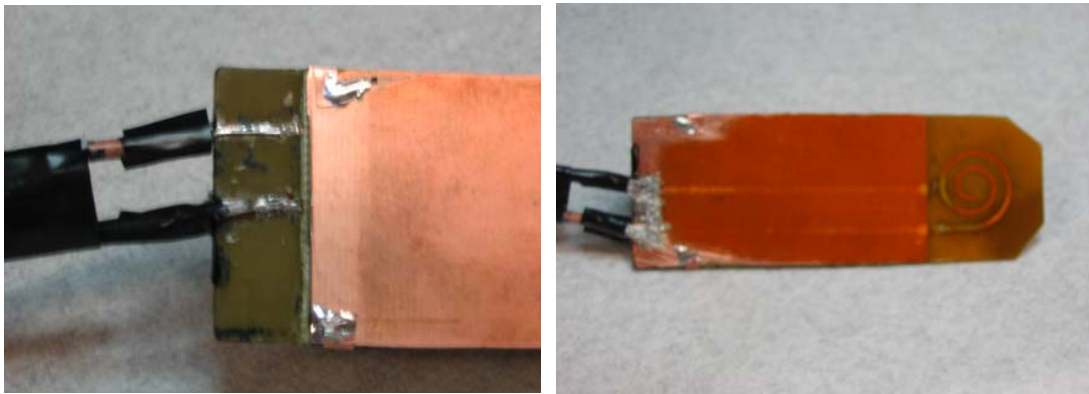


Fig. 38: The sensor feed structure and the completed sensor

Although the sensor was designed to transmit pulses, technical constraints limited the testing of the sensor to swept frequencies from the VNA (see Chapter Three). The sensor's response to pulses and swept frequencies should be very similar. To verify that the sensor response was affected by changes in permittivity, materials with various dielectric constants were placed on the sensor and its response was measured.

The first test involved low dielectric materials: air ($\epsilon' = 1$), ultem ($\epsilon' = 6$), ceramic tile ($\epsilon' = 10$). As is seen in Figure 39, a dielectric constant change from 1 to 6 (air to ultem) yielded a 56 MHz shift in the $|S_{21}|$ plot at 1 GHz, and a dielectric constant change from 1 to 10 (air to tile) yielded a 145 MHz shift in the $|S_{21}|$ plot at 1 GHz. Additionally,

greater frequency shifts were seen at higher frequencies (168MHz and 331MHz respectively centered around 1.66 GHz).

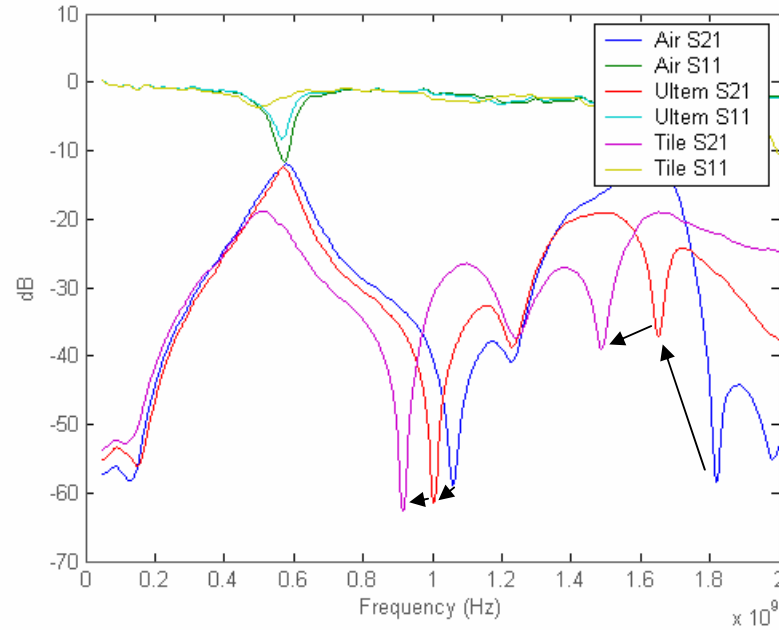


Fig. 39: $|S_{11}|$ and $|S_{21}|$ for air, ultem, and tile

To evaluate the performance of the sensor at higher dielectrics, plastic bags of water were placed on the sensor. One bag contained 23.6 °C water (measured by a K-type thermocouple), and the other was 47.3 °C. On the $|S_{21}|$ plot, a maximum at 1.35 GHz shifted 74 MHz and a minimum at 1.9 GHz shifted 126 MHz. It is important to note that at these higher permittivity values, the $|S_{21}|$ signal appears to be much stronger than it was during the air, ultem, tile test. Additionally, the resonant frequency at 1.55 GHz in the $|S_{11}|$ moved 93 MHz (see Fig. 40). Based on these results, it is obvious that the sensor is behaving in the manner initially sought after in Chapter Six. Specifically, the $|S_{11}|$ and $|S_{21}|$ both respond to changes in permittivity of the MUT.

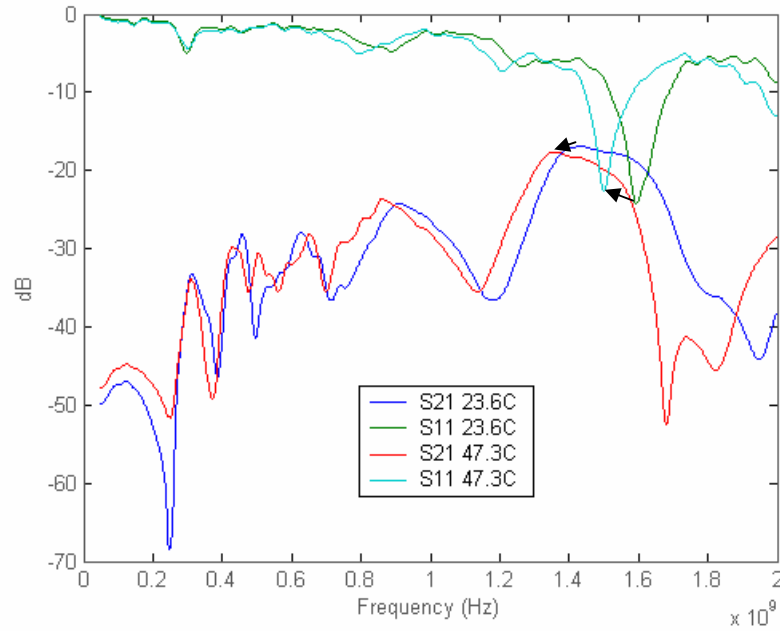


Fig. 40: $|S_{11}|$ and $|S_{21}|$ for various temperatures of water

The single-spiral microstrip resonant sensor has been shown to work for high and low dielectrics. But, it has not yet been shown to be capable of measuring the complex response of biological tissues. To test this feature of the antenna, samples of ground beef were prepared by mixing fatty beef with lean beef in a food processor. Each sample had a different fat content, ranging from 4% to 25%. The sensor's response indicated that the sensor was able to resolve changes in fat content (see Fig. 41 and Fig. 42). As was described in Chapter Five, meat with higher fat content has less water and therefore a lower dielectric constant. As fat content varies, the $|S_{11}|$ plot has a 115 MHz shift in frequency centered at 780 MHz. In the $|S_{21}|$ plot, there is a 110 MHz frequency shift centered at 1.16 GHz. The sensor has demonstrated that it can operate over a range of permittivities as well as measure biological tissues.

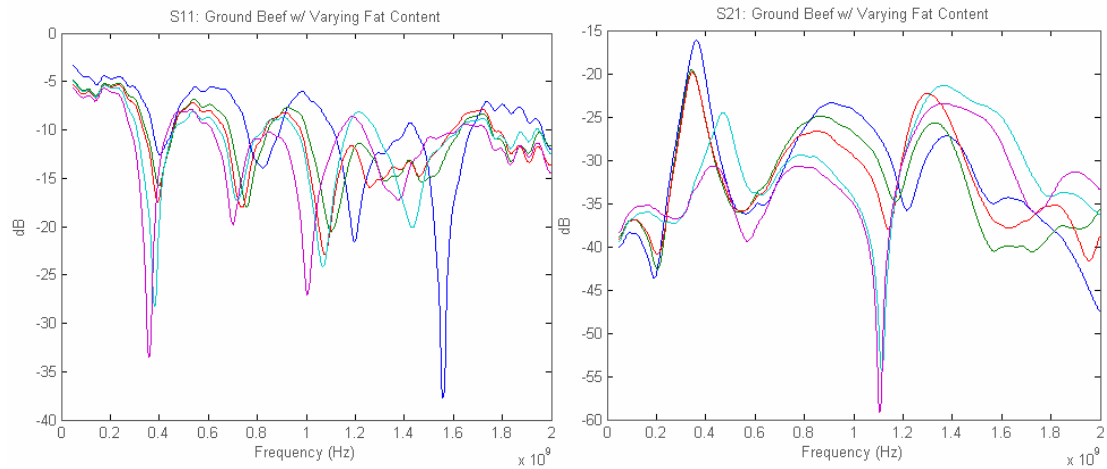


Fig. 41: $|S_{11}|$ and $|S_{21}|$ response of sensor loaded with meat

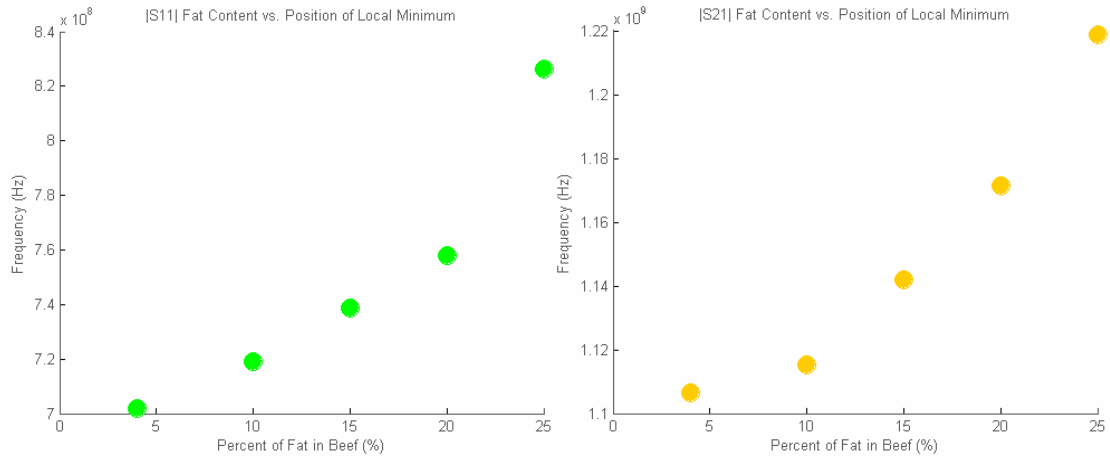


Fig. 42: Tracking a local minimum vs. fat content in $|S_{11}|$ and $|S_{21}|$

The final test to see whether the single-spiral microstrip resonant sensor may be used to determine blood glucose concentration is the “soda test.” The soda test consists of someone fasting for at least eight hours. Then, the antenna is placed on a part of the body with a lot of blood (i.e., the volar part of the wrist as in Figure 43). The sensor may be held in place by hand, but the lack of constant pressure will slightly affect the results. After taking several measurements with the sensor, the user rapidly drinks a sugared soda. Once the drink is consumed, data should be taken for at least an hour. As with the

other test cases, permittivity changes in the MUT will show up as shifts in frequency of the maximums and minimums in the sensor's $|S_{11}|$ and $|S_{21}|$ plots.



Fig. 43: Sensor located at the wrist measuring-site

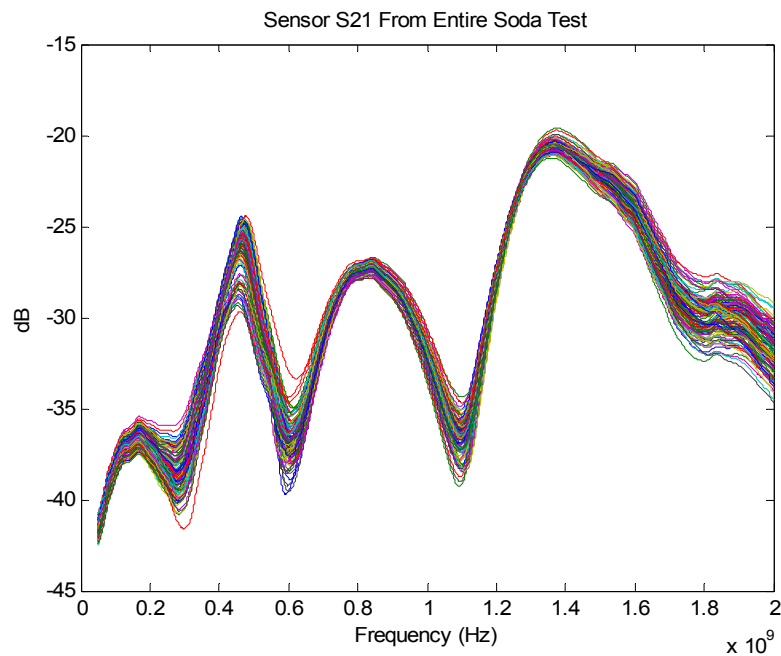


Fig. 44: $|S_{21}|$ plots from each measurement taken over the duration of the soda test

Once all the data is taken, a plot similar to Figure 44 may be generated. From this plot, maximums and minimums are selected, and their frequency can be observed over time. Numerous peaks and nulls are able to be tracked. From the experimental data, most maxima and minima in the plot show some behavior relating to the consumption of

the soda. The best examples from the data are illustrated in Figure 45 and Figure 46. The yellow line is the raw data, which was processed with a five-point moving average to produce the red and blue lines. The red line in these figures corresponds to measurements taken prior to consumption of the soda. The blue line corresponds to measurements taken after consumption of the soda. The green line is the best-fit polynomial to the yellow data.

Since the red measurements were taken before the soda was consumed, it logically follows that this line should be relatively constant. Unfortunately, this is not so. Pre-drinking peak movement may be due to inconsistencies in pressure holding the antenna on the skin. If there is any air between the sensor and the skin, the sensor's response will not be accurate. Also, the non-flat region of the red curve may be a result of the cephalic phase of insulin secretion, which occurs when insulin release is triggered merely by the smell, sight, or even thought of food, rather than consumption [43]. This could cause premature changes in glucose levels by triggering action of the body's standard glucose regulation mechanisms. Despite the non-flatness of the red region, the blue region in Figure 45 clearly exhibits a response to the consumption of the soda. When glucose levels are spiked, there is a steady rise in glucose concentration and then a rapid drop-off when insulin secretion occurs; the blue curves indicate that the sensor is likely measuring this rise and drop-off.

A resonant sensor has been designed whose response is a function of permittivity. It has been shown that the permittivity of human tissues changes after sugar is consumed, most likely a result of changes in blood permittivity. Whether the parameter actually being sensed is related to blood glucose or some other biological mechanism remains to

be seen, but that is not within the scope of this thesis.

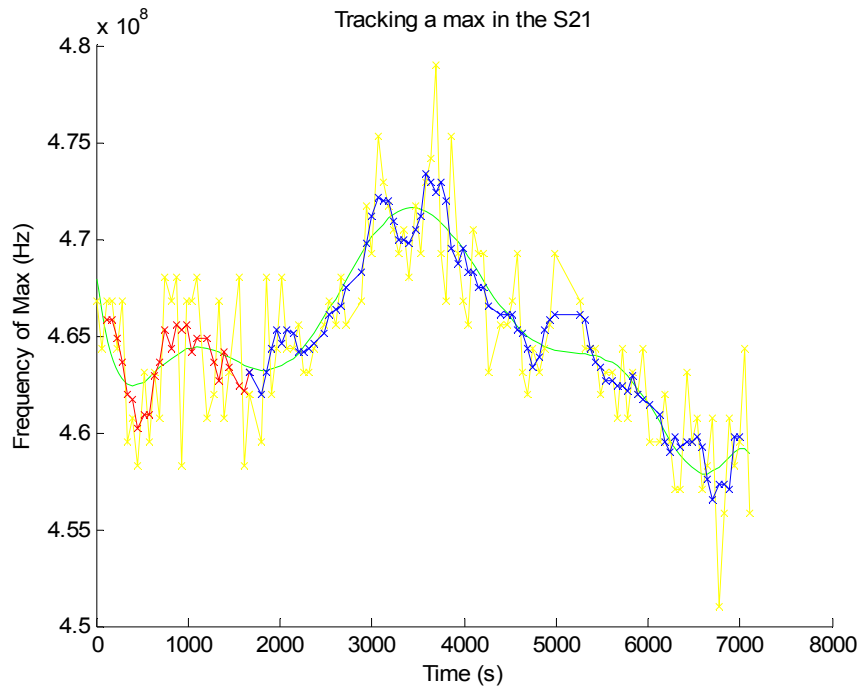


Fig. 45: Tracking a maximum of the $|S_{21}|$ over time

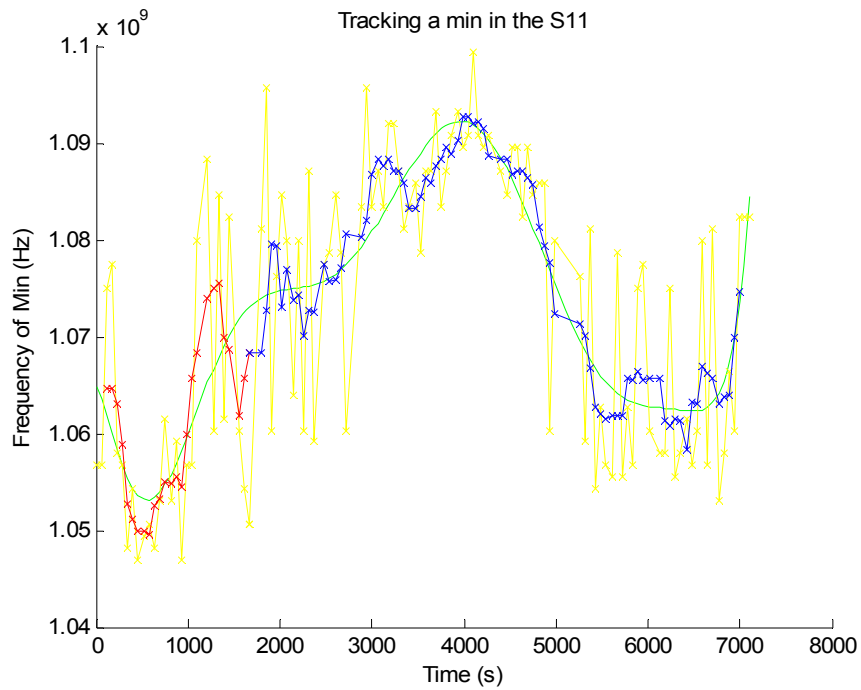


Fig. 46: Tracking a minimum of the $|S_{11}|$ over time

CHAPTER EIGHT

Final Recommendations and Description for Development of a Non-Invasive Glucose Meter

A single-spiral microstrip resonant sensor has been designed and shown to exhibit significant changes in its response resulting from changes in permittivity of the material under test (MUT). The sensor is able to detect these changes non-destructively and non-invasively, without making direct contact with the MUT. Initial results suggest that this sensor is capable of measuring physiological responses that result from changing levels of blood glucose. If this is true, the single-spiral microstrip resonant sensor may become the heart of the first truly non-invasive glucometer that diabetics can use on a daily basis.

While a considerable amount of effort went into the design of the sensor, more may be done to improve its performance as a glucose monitor. Once further research has been performed into the dielectric properties of blood at microwave frequencies, sensor parameters such as number of turns, trace width, gap size, and substrate thickness can be refined. This would allow the sensor to be tuned to glucose concentration in a manner simply not achievable without further study.

Additionally, if the sensor were on flexible circuit material similar to the slotline bowtie described in Chapter Four, a better match to the contours of the measuring-site may be achievable. This would permit more of the signal to enter the body and a better sensor response. In its current implementation, thinning the sensor down so that it would be flexible would require narrower traces and a higher substrate dielectric constant.

If the sensor is developed into a fully functional microwave glucometer, there are several methods which may be used to turn the sensor output into a meaningful measurement. However, before these methods can be explored, more needs to be known about what exactly the sensor is measuring. Blood has numerous constituents, all of which may vary in concentration between individuals, and even from day to day in the same individual. In order to design a glucometer, these parameters effect on blood's permittivity, and thus the sensor's response, need to be more clearly understood. It may be that a microwave glucometer has to be recalibrated periodically by a physician or against an invasive glucometer to account for these effects.

Another barrier to development of a microwave glucometer is the variability of specific physiological parameters between individuals. These parameters include, skin thickness, body fat percentage, water content, blood flow, tissue density, and blood volume at the measuring site. However, in Chapter Four microwave thermography was presented as a method for measuring many of these parameters. It may be that through implementation of multiple microwave sensors measuring various parameters, a single calibration for a microwave glucometer, applicable to all users, may be obtained.

Microwave sensors are robust and economical and pose a very elegant solution to the problem of invasive glucose testing. Specifically advantageous is their ability to measure permittivity without physically contacting the sample. While it is clear that the development of a microwave glucometer will take some time, the promising results demonstrated in Chapter Seven indicate that a single-spiral microstrip resonant sensor may be the key to the device's future.

BIBLIOGRAPHY

- [1] E. Nyfors and P. Vainikainen, *Industrial Microwave Sensors*, 1989.
- [2] E.C. Green, "Proposed Method for Non-Invasive Measurement of Blood Glucose Concentration: Using Microwaves for Data Measurement and Analysis," Dec. 2004.
- [3] W.J. Germann and C.L. Stanfield, *Principles of human physiology*, San Francisco: Benjamin Cummings, 2002.
- [4] T. Smith, "Our Deadly Diabetes Deception," *Nexus Magazine*, vol. 11, June – July 2004.
- [5] W/ Davis, "Direct & Indirect Costs of Diabetes in the United States," American Diabetes Association, Feb 18, 2004. Accessed Oct. 20, 2005. Available HTTP: <http://www.diabetes.org/diabetes-statistics/cost-of-diabetes-in-us.jsp>.
- [6] Norman Endocrine Surgery Clinic, "Normal Regulation of Blood Glucose," Norman Endocrine Surgery Clinic, 2002. Accessed Oct. 20, 2005. Available HTTP: <http://www.endocrineweb.com/insulin.html>.
- [7] Burke, Dr. Edmund R., "Hitting the Wall: What Causes Muscle Fatigue?" *Muscular Development*, November, 1999.
- [8] National Diabetes Information Clearinghouse, *Diagnosis of diabetes*, Bethesda, Md.: National Institute of Diabetes and Digestive and Kidney Diseases, National Institutes of Health, U.S. Dept. of Health and Human Services, 2004.
- [9] "Review Criteria Assessment of Portable Blood Glucose Monitoring In Vitro Diagnostic Devices Using Glucose Oxidase, Dehydrogenase or Hexokinase Methodology (Draft Version)," U.S. Food and Drug Administration Center for Radiological Health, Feb. 28, 1997. Accessed Apr. 22, 2005. Available HTTP: <http://www.fda.gov/cdrh/ode/gluc.html>.
- [10] "Forearm blood samples yield accurate results in home blood glucose monitors," *Diabetes Week*, pp. 17, November 8, 2003.
- [11] Harvard Medical School, "Harvard Heart Letter," EBSCO Publishing and Gale Group, pp. 5-6, October 2001.
- [12] "FDA Approves GlucoWatch Device for Children with Diabetes," FDA News, Aug. 27, 2002. Accessed Apr. 22, 2005. Available HTTP: <http://www.fda.gov/bbs/topics/NEWS/2002/NEW00830.html>.

- [13] S. Halasey, "Next-Generation Diagnostics: Big, Small, and Fast," *Medical Device & Diagnostic Industry Magazine*, April, 1999. 1999.
- [14] United States, *United States frequency allocations*, Washington, DC: U.S. Dept. of Commerce, National Telecommunications and Information Administration, Office of Spectrum Management, 2003.
- [15] L.C. Shen and J.A. Kong, *Applied Electromagnetism*, Boston, MA: PWS Publishing Company, 1995.
- [16] D.M. Pozar, *Microwave Engineering, 3rd Edition*, United States: John Wiley & Sons, 2005.
- [17] J.P. Grant, R.N. Clarke, G.T. Symm and N.M. Spyrou, "In vivo dielectric properties of human skin from 50 MHz to 2.0 GHz," *Phys.Med.Biol.*, vol. 33, pp. 607-612, 1988.
- [18] M.S. Venkatesh and G.S.H. Raghavan, "An overview of dielectric properties measuring techniques," *Canadian Biosystems Engineering*, vol. 47, pp. 7.15-7.30, May 13, 2005. 2005.
- [19] Agilent Technologies, "Agilent 85070E Dielectric Probe Kit 200 MHz to 50 GHz Technical Overview," Agilent Technologies., November 6, 2003, 2003.
- [20] K. Chang, *Microwave Ring Circuits and Antennas*, New York: John Wiley and Sons, 1996.
- [21] "IEEE standard for safety levels with respect to human exposure to radio frequency electromagnetic fields, 3 kHz to 300 GHz," *IEEE Std C95.1, 1999 Edition*, 1999.
- [22] A.W. Guy, "History of Biological Effects and Medical Applications of Microwave Energy," *Microwave Theory and Techniques, IEEE Transactions on*, vol. 32, pp. 1182-1200, 1984.
- [23] H.P. Schwan, "Interaction of Microwave and Radio Frequency Radiation with Biological Systems," *Microwave Theory and Techniques, IEEE Transactions on*, vol. 19, pp. 146-152, 1968.
- [24] B. Stec, A. Dobrowolski and W. Susek, "Estimation of temperature distribution inside biological tissues by means of multifrequency microwave thermograph," 2001, pp. 3901-3903 vol.4.
- [25] M. Kaczmarek, A. Nowakowski, A. Renkielska, J. Grudzinski and W. Stojek, "Investigation of skin burns basing on active thermography," 2001, pp. 2882-2885 vol.3.

- [26] Y. Kim and Y. Cho, "Correlation of pain severity with thermography," 1995, pp. 1699-1700 vol.2.
- [27] B. Wiecek and S. Zwolenik, "Thermal wave method - limits and potentialities of active thermography in biology and medicine," 2002, pp. 1133-1134 vol.2.
- [28] A. Rosen, M.A. Stuchly and A.V. Vorst, "Applications of RF/microwaves in medicine," *Microwave Theory and Techniques, IEEE Transactions on*, vol. 50, pp. 963-974, 2002.
- [29] E.C. Fear, X. Li, S.C. Hagness and M.A. Stuchly, "Confocal microwave imaging for breast cancer detection: localization of tumors in three dimensions," *Biomedical Engineering, IEEE Transactions on*, vol. 49, pp. 812-822, 2002.
- [30] S.C. Hagness, A. Taflove and J.E. Bridges, "Three-dimensional FDTD analysis of a pulsed microwave confocal system for breast cancer detection: design of an antenna-array element," *Antennas and Propagation, IEEE Transactions on*, vol. 47, pp. 783-791, 1999.
- [31] S.C. Hagness, A. Taflove and J.E. Bridges, "Wideband ultralow reverberation antenna for biological sensing," *Electronics Letters*, vol. 33, pp. 1594-1595, 1997.
- [32] G.B. Gentili, V. Tesi, M. Linari and M. Marsili, "A versatile microwave plethysmograph for the monitoring of physiological parameters," *Biomedical Engineering, IEEE Transactions on*, vol. 49, pp. 1204-1210, 2002.
- [33] R. Pethig, "Dielectric properties of body tissues," *Clinical Physics and Physiological Measurement*, vol. 8, pp. 5-12, 1987.
- [34] N.K. Gupta, S.K. Srivastava and H.V. Tiwari, "Estimation of Emissivity Characteristics of Biological Tissues at Microwave Frequency," *IE(I) Journal-ID*, vol. 84, pp. 1-2-3, May 2004. 2004.
- [35] S.S. Seker, G. Apaydm and M. Kuzu, "Comparison of electrical parameters of human body parts with vegetation," 2003, pp. 3241-3244 Vol.4.
- [36] O.G. Martinsen, S. Grimnes and H.P. Schwan, "Interface Phenomena and Dielectric Properties of Biological Tissue," in *Encyclopedia of Surface and Colloid Science*, Marcel Dekker, Inc., 2002, pp. 2643-2643-2652.
- [37] C.M. Alabaster and Dahele, Professor J. S. (supervisor), "The Microwave properties of tissue and other lossy dielectrics," Cranfield University; College of Defence Technology; Department of Aerospace, Power and Sensors, July 1, 2004.
- [38] S. Gabriel, R.W. Lau and C. Gabriel, "The dielectric properties of biological tissues: III. Parametric models for the dielectric spectrum of tissues," *Phys.Med.Biol.*, vol. 41, pp. 2271-2293, 1996.

- [39] B.R. Jean, "Guided Microwave Spectrometry for In-line Analysis of Flowable Materials," in *RF & Microwave Sensing of Moist Materials, Food, and other Dielectrics*, vol. 7, K. Kupfer, A. Kraszewski and R. Knochel Eds. Weinheim: Wiley, 2001,
- [40] Y. Hayashi, L. Livshits, A. Caduff and Y. Feldman, "Dielectric spectroscopy study of specific glucose influence on human erythrocyte membranes," *J.Phys.D*, vol. 36, pp. 369-374, 2003.
- [41] J. Park, C. Kim, B. Choi and K. Ham, "The correlation of the complex dielectric constant and blood glucose at low frequency," *Biosensors and Bioelectronics*, vol. 19, pp. 321-324, 12/15. 2003.
- [42] A. Caduff, E. Hirt, Y. Feldman, Z. Ali and L. Heinemann, "First human experiments with a novel non-invasive, non-optical continuous glucose monitoring system," *Biosensors and Bioelectronics*, vol. 19, pp. 209-210-217, May 15, 2003.
- [43] V. Seshiah and C.V. Harinarayan, "Insulin Kinetics," *Int. J. Diab. Dev. Countries*, vol. 18, pp. 19-20-22, 1998.